Structural studies of Quartzo-Feldspathic veins from parts of North-Odisha Singhbhum Craton: Special reference to Paleo-stress Analysis

Thesis submitted to

Indian Institute of Science Education and Research, Pune

in the partial fulfilment of the award of the degree

Of

Master of Science

In

Geology

By

Gopinatha Nayak

(20226404)

Under the supervision of

Dr. Durga Prasanna Mohanty

Department of Earth and Climate Science

Indian Institute of Science Education and Research

Pune, 411008

Session: 2022-24

भारतीय विज्ञान शिक्षा एवं अनुसंधान संस्थान पुणे
INDIAN INSTITUTE OF SCIENCE EDUCATION AND RESEARCH PUNE
An Autonomous Institution of the Ministry of Education, Govt. of India

CERTIFICATE

This is to certify that the thesis entitled **"Structural studies of qurtzo-feldspathic veins from parts of North-Odisha Singhbhum Craton: Special reference to Paleo-stress analysis"**, towards the fulfilment of the degree of Master of Science in Geology programme at the Indian Institute of Science Education and Research, Pune, represents study/work carried out by **Mr. Gopinatha Nayak (20226404)** at Savitribai Phule Pune University, under the supervision of **Dr. Durga Prasanna Mohanty,** Assistant Professor, Department of Geology, Savitribai Phule Pune University, during the academic year 2023-2024.

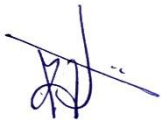

Dr. Durga Prasanna Mohanty
Assistant Professor
Department of Geology
Savitribai Phule Pune University,
411007

DECLARATION

I hereby declare that the work presented in the thesis is original and has been done under the guidance of my supervisor. The work has not been submitted to any other institute for any degree or any diploma. I have followed the guidance provided by the Institute in writing the thesis and have confirmed to the ethical norms and guidelines of the Institute while writing the thesis. Whenever I have used any materials like figures, maps, models or data from other external sources, I have given due citing them in text with their details in references.

Gopinatha Nayak

Gopinatha Nayak

(20226404)

ACKNOWLEDGEMENT

I want to extend my heartfelt gratitude to my supervisor Dr. Durga Prasanna Mohanty, Assistant Professor, Department of Geology, Savitribai Phule Pune University for his valuable guidance, constant support, and encouragement throughout this project. I have greatly benefited from his experience and criticism in refining my concepts and raising the Caliber of my work.

I am grateful to my thesis expert, Dr. Sudipta Sarkar for his feedback and constructive criticism during my mid-term evaluation which helped me to learn more things related to my research and strengthen my arguments.

I would like to express my deepest gratitude to Mr. Bishuddhakshya Puhan and Mr. Rakesh for his constant help, suggestions and support while working on this project.

And finally, I thank my family and friends who have supported me emotionally and provided encouragement throughout this journey. Their unwavering support has been a source of motivation and inspiration.

Gopinatha Nayak

Gopinatha Nayak

(20226404)

List of Figures

Fig 1.1 Generalized geological and tectonic map of the Indian sub-continent with the Precambrian mafic dyke swarms cross-cutting various Archean Cratonic blocks. C: Cuddapah basin; Chhattisgarh basin; CITZ: Central Indian Tectonic Zone; GR: Godavari Rift; M: Madras Block; Mk: Malanjkhand; MR: Mahanadi Rift; N: Nilgiri Block; NS: Narmada-Son Fault Zone; PC: Palghat-Cauvery Shear Zone; R: Rengali Province and Kerajang Shear Zone; S: Singhbhum Shear Zone; V: Vindhyan Basin. Source: (modified after French et al., 2008).

Fig 1.2 Superimpose of Singhbhum craton formation map over Google Earth Pro and have added the placemarks in field locations (Balushi et al., 2022).

Fig 3.1 Diagrammatic two-dimensional illustration of a planar discontinuity opening with normal stress on its walls exceeded by pore fluid pressure (P_f) at a certain.

Fig 3.2 The maximum principal stress (σ_n), maximum shear stress (τ_{max}), and minimum principal stress (σ_3), are displayed on a Mohr circle construction. Plotting the fluid pressure (P_f) along the normal stress (σ_n) axis is done. Because the usual stress is lower than the fluid pressure, fractures in the shaded area to the left of the fluid pressure line can enlarge. It is not possible for fractures to enlarge to the right of the fluid pressure line. The triangle FOC determines the opening direction (μ) of a fracture, and the triangle AOB is utilized to calculate the R ratio (Jolly and Sanderson, 1997).

Fig 3.3 orientation of σ_1, σ_2, and σ_3 as determined from the quartz vein's girdle distribution, while θ_2 and θ_3 are determined from the ellipse.

Fig 4.1 Satellite image of locations visited

Fig 4.2 Field photographs of Quartz vein in Singhbhum granite of Anandpur region is showing extensional veins (a) Pegmatite veins clearly visible on google earth pro satellite image orienting N-S (b) In the image, the first phase of the N-S oriented plagioclase-rich pegmatite vein intersects with the later phase of the NE-SW oriented pegmatite vein. (c) NW-SE oriented curved quartz vein in exfoliated granite (d) The first phase of NW-SE oriented quartz vein is intersecting the later phase of N-S oriented quartz vein which created an offset in the first phase quartz vein (e) Three sets of orienting NW-SE, NE-SW and E-W are intersecting each other in granite hosted

rock (f) NE-SW oriented quartz vein is intersects with the later phase of N-S oriented pegmatite veins

Fig 4.3 (a) In the image, the first phase of the NE-SW oriented quartz vein intersects with the later phase of the NW-SE oriented quartz vein. (b) Quartz vein in granitic hosted rock showing gradational contact with the host rock. (c) Three sets of quartz veins orienting N-S, NE-SW and NW-SE are intersecting each other at a common point. (d) Conjugate sets of quartz veins orienting N-S and E-W are intersecting each other and showing some degree of offset. (e) Feldspar clearly showing 2 sets of cleavage. (f) Two sets of conjugate fracture planes orienting N-S and E-W are intersecting each other and showing offsets.

Fig 4.4 Intense brittle deformation has occurred in this area (a) A fracture having space around 15 cm is conjugately intersecting with another fracture having space around 5 cm. (b) Two conjugate pegmatite veins are intersecting each other having thickness around 15 cm. (c) The early phase SE-NW oriented fracture plane is intersecting the later phase of NE-SW oriented fracture plane and offset has formed. (d) The N-S oriented fracture plane is intersecting with the E-W oriented fracture plane and offset has formed in well foliated gneissic host rock. (e) Three sets of fracture planes are intersecting each other and resulting a triangular shape structure in gneissic host rock. (f) A quartz vein orienting NW-SE intersecting with NE-SW fracture plane.

Fig 4.5: Megascopic and thin section study (a) Showing N-S and NE-SW oriented pegmatitic veins (b) Sample taken from pegmatitic vein in (a) and showing big grains of plg and feldspar (c) Conjugate quartz veins (d) sample taken from quartz vein in (c) showing big grains of qtz (e) Showing thin section of host granite rock.

Fig 5.1 (a) Rose diagram of fractures data of Anandpur region which shows the most number of fractures are trending NE-SW. (b) Rose diagram of veins data of Anandpur region which shows NE-SW tend similar to the fractures.

Fig 5.2 Rose diagram of fractures data of Bhimkund region which shows a general trend towards NE-SW.

Fig 5.3 (a) Contour plot of all veins with the best fit ellipse drawn in the free space (b) Poles to veins with the best fit ellipse (c) 3D Mohr circle showing the relative stress value and the relation between pore fluid pressure and principal stresses.

List of Tables

Table 1 showing the stratigraphic sequence of Singhbhum Craton from Paleo Mesoarchean (after Saha 1994 and Ghosh et al., 2019)

Table 2 Field data sets with location

CONTENTS

	Page No.
Certificate	2
Declaration	3
Acknowledgment	4
List of Figures	5
List of Tables	7
Abstract	9
1. Introduction	10
1.1 Introduction	10
1.1.1 Dharawar Craton	10
1.1.2 Baster Craton	10
1.1.3 Singhbhum Craton	10
1.1.4 Aravali Craton	10
1.1.5 Bundelkhand Craton	11
1.2 Singhbhum Craton	13
1.3 General Geology	13
1.3.1 Veins and Fractures	16
1.4 Literature Review	17
1.5 Study Area	19
1.5.1 Location	19
1.5.2 Physiography and Accessibility	19
1.5.3 Geology of the Study area	20
2. Research gap and Objectives of study	22
2.1 Research gap	22
2.2 Objectives	22
3. Methodology	23
3.1 Field data acquisition and Sample collection	23
3.2 Lithological Map preparation	24
3.3 Paleostress analysis method	24
3.3.1 Fault slip analysis	24
3.3.2 Fractures and Veins analysis	25

3.3.3 Numerical modelling 25
3.3.4 Integrated approach 25
3.4 Theoretical concept 26
3.4.1 Fracture opening condition 27
3.4.2 3D Mohr circle construction 29
4. Structural analysis 32
4.1 Fieldwork 32
5. Result and Discussion 50
5.1 Result and Discussion 50
5.2 Conclusion 54
References 55

ABSTRACT

Singhbhum Craton in Peninsular India is one of the oldest Archean Craton that preserves the history and signature of the early continental crust. It preserves the records of several episodes of volcanism, sedimentation, and metallogenic processes from Palaeoarchean to the Mesoproterozoic. It is traversed by Singhbhum Shear Zone (SSZ). The shear zone separates a northern terrain of more highly metamorphosed rocks and a southern terrain of relatively less metamorphosed rocks.

Anandpur area is a part of southern Singhbhum craton which is mostly dominated by Singhbhum Granite (SG) and Older Metamorphic Tonalite Gneiss (OMTG). These are present as enclaves or pockets within singhbhum granites. Granitic bodies are intruded by quartz and pegmatite veins. Pegmatite is intruded in the country rock in numerous places showing possibility of hydrothermal alteration in country rock due to pegmatite intrusion.

The emplacement of quartz and pegmatite veins into the fracture plane is controlled by both pore fluid pressure (P_f) and normal stress (σ_n). By plotting the orientations of veins and fractures which are collected from the field in stereonet and Mohr plotter, pore fluid pressure and tectonic stress ratio are measured. Total 235 quartz veins and 65 fracture planes orientations are measured and the most noticeable direction is NE–SW. Although veins are cross cutting each other, it's proven from the field photos that they are synchronous. In the stereoplot poles to the veins displays a girdle distribution pattern with an elliptical gap region in the middle of it and the plane striking N30°E represents σ_1-σ_2 plane. Further, θ_2 and θ_3 value is 17° and 34° respectively, and the trend and plunge amount of σ_1, σ_2 and σ_3 is 075° / 81.5°, 210° / 06° and 300° / 06° respectively, which represents maximum expansion in NW-SE. The stress ratio (ϕ) and the driving pressure ratio (R') are calculated as 0.72 and 0.91 respectively, high value of driving ratio represents broad range of fractures to dilate and the high φ value indicating uniaxial extension. 3D Mohr plot shows the variation of fluid pressure in between σ_1 and σ_2.

CHAPTER 1

INTRODUCTION

1.1 Introduction

Craton is a stable interior part of the continent that suffers little deformation. They consist of pre-Cambrian basement rocks overlain by a sedimentary cover. The basement rocks (10-12km thick) are highly deformed and metamorphosed compared to the sedimentary cover. Cratons are the Archean formations whose traces can be seen in many parts of our country. There are 5 major cratons present in India, such are Dharwar craton, Baster craton, Singhbhum craton, Aravalli and Bundelkhand craton.

1.1.1 Dharwar Craton

One of the biggest and oldest cratonic blocks on Earth (~3.4 Ga) is the Dharwar craton of the Indian shield (Mandal et al.,2017). The Dharwar craton is rich in economic mineral deposits like gold and copper.

1.1.2 Baster Craton

Baster craton is the central Indian craton which has rich mineral deposits of manganese, Iron, copper, etc. The Proterozoic orogenic belts that make up the Eastern Ghats Mobile Belt and the Central Indian Tectonic Zone (the Satpura Mobile Belt) border the southeastern and northern borders of the craton respectively. (Mohanty, 2021)

1.1.3 Singhbhum Craton

One of the oldest Archean cratons that still possesses the signature and history of the early continental crust is the Singhbhum Craton in Peninsular India. It keeps the records of several metallogenic processes, sedimentation, and volcanism occurrences from the Paleoarchean to the Mesoproterozoic era. The Singhbhum Shear Zone (SSZ) passes through it which divides the southern terrain with comparatively less metamorphosed rocks from northern terrain with more heavily metamorphosed rocks.

1.1.4 Aravalli Craton

The Precambrian core of northwest India is represented by the Aravalli Craton, which is made up of the Archean Banded Gneissic Complex (BGC; 3.3–2.5 Ga) (Ghosh et al., 2022). It's a unique craton on the basis of absence of greenstone belt and rich in economic minerals like lead and zinc.

1.1.5 Bundelkhand Craton

Bundelkhand craton is the smallest craton among the major five cratons and it lies towards northern part of India bounded by (Central Indian Tectonic Zone) CITZ in the southern boundary.

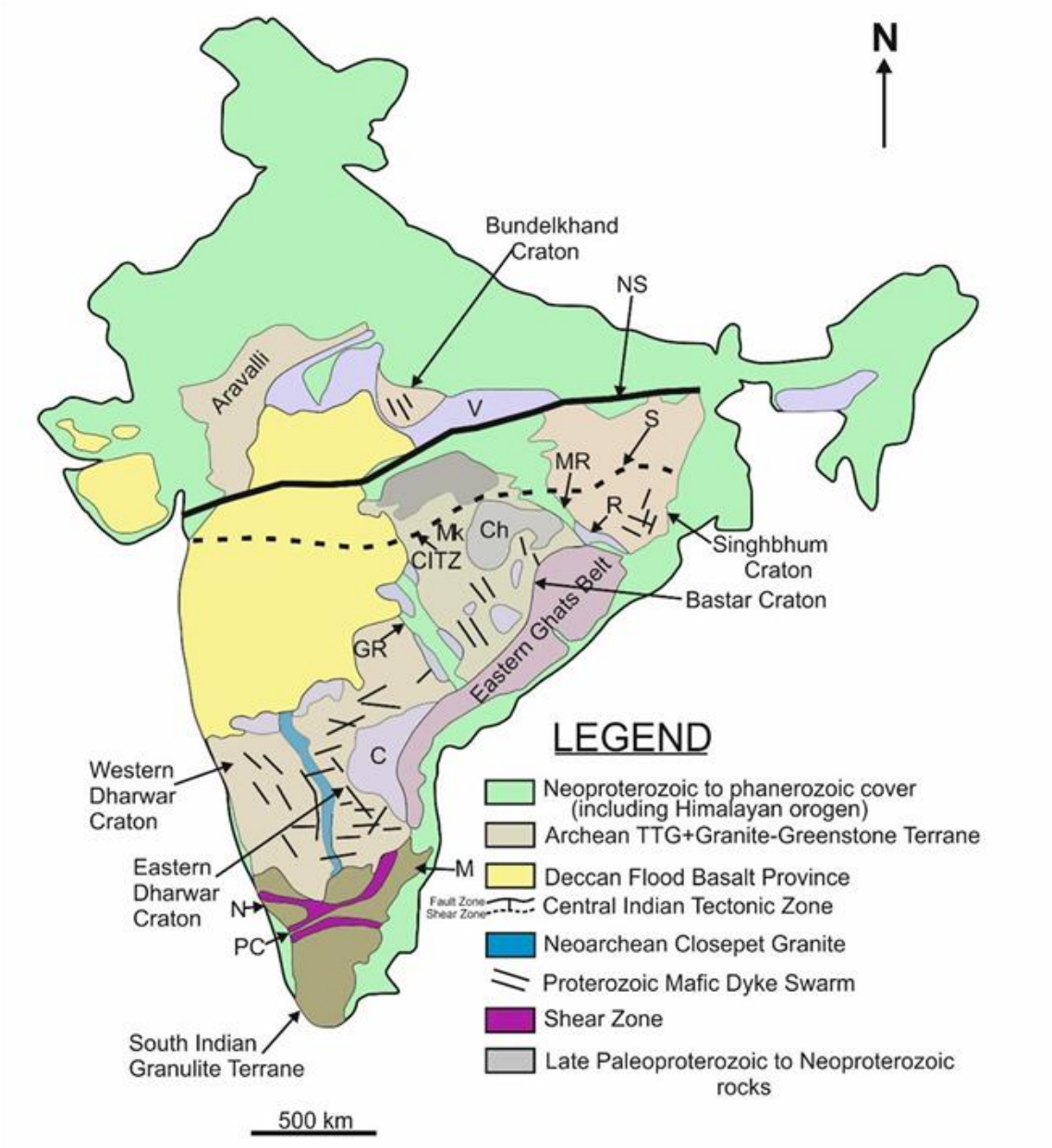

Fig.1.1 Generalized geological and tectonic map of the Indian sub-continent with the Precambrian mafic dyke swarms cross-cutting various Archean Cratonic blocks. C: Cuddapah basin; Chhattisgarh basin; CITZ: Central Indian Tectonic Zone; GR: Godavari Rift; M: Madras Block; Mk: Malanjkhand; MR: Mahanadi Rift; N: Nilgiri Block; NS: Narmada-Son Fault Zone; PC: Palghat-Cauvery Shear Zone; R: Rengali Province and Kerajang Shear Zone; S: Singhbhum Shear Zone; V: Vindhyan Basin. Source: (modified after French et al., 2008)

1.2 Singhbhum craton

Singhbhum craton exposes some oldest rock formations of India. Singhbhum Craton lies in between 2 Proterozoic mobile belts- Satpura Mobile Belt in the north and north-west; Eastern Ghat Mobile Belt in the south. It is separated from Bastar Craton by Mahanadi Graben. The south of singhbhum craton and Eastern Ghat Mobile Belt (EGMB) has a tectonic contact marked by Sukinda Shear zone (Mukhopadhyay, Dhruva and Matin,2020). Eastern side is bounded by marine sediments of Bay of Bengal. It covers arounds 40,000 sq. km.

It is positioned in northern elements of Odisha and Jharkhand states. It appears as an oval block trending N-S between the coordinates of 84.5°E and 86.5°E and 21°N to 22.75°N. The whole region is dissected by Singhbhum Shear Zone (SSZ). The shear zone separates a northern terrain of fairly metamorphosed rocks and a southern terrain of relatively less metamorphosed rocks. The craton is made up of various supracrustal sequences and granitoid rocks (3.5 to 2.5 Ga.) (Mukhopadhyay, 2001; Sarkar and Gupta, 2012). The Singhbhum granite is a craton core (8000 km²) surrounded by supracrustal of various ages and characteristics. The Singhbhum orogen has an arcuate shape and wraps around the Singhbhum granite to the north. Copper mineralization is linked to the Copper belt shear zone, which may be found on the granite's northern border.

1.3 General geology

An oval-shaped Archean cratonic core in the Singhbhum region is flanked to the north (NSMB) and south (SMB) by Proterozoic mobile belt rocks (Rengali Province, RP). The Archean cratonic core's northern boundary with the RP is marked by the Singhbhum Shear Zone (SSZ), while its southern boundary with the RP is marked by the crustal-scale Sukinda thrust-Barkot Shear Zone. The following are the main components of the Archean cratonic core of the Singhbhum region:

1. Older Metamorphic Tonalite Gneiss (OMTG), Singhbhum Granite (SBG), Bonai Granite, and Mayurbhanj Granite are all part of the gneissic and granitoid suite.
2. The Older Metamorphic Group (OMG) and Iron Ore Group (IOG) rocks, belong to an older supracrustal sequence.

3. Dhanjori Group and equivalents (Simlipal Group, Mahagiri Formation, and Keonjhar Formation), which are younger supracrustal sequences.
4. Gabbro-anorthosite and Newer Dolerite dyke swarms comprise an intrusive mafic ultramafic suite.

OMG's largest region is Champua, which has 200 square kilometres of enclaves; other placeless include Shankarpur, Onlajodi, Bahalda, and Huludpukhur (Saha et al., 1988). The most common rock types include biotite-muscovite schist, quartzite, fuchsite quartzite, orthoambhibole, schistose iron deposit, sphene, rutile, and zircon. Regional foliation trends vary from ENE to ENE. The Sm-Nd (WR) isochrones in OMG amphibolite has a 3300Ma age and a Pb-Pb age of 3380Ma.

The Older Metamorphic Tonalite Gneiss (OMTG) is found in Champua, Seraikala, Onlajodi, Rairangpur, and Thakurmunda and covers an area of around 900 square kilometres (Saha, 1994). The most prevalent rock type is tonalite-trondhjemite-granodiorite, with quartz diorite and monzodiorite as minor components. The gneisses contain a lot of Sr, have a low Ba/Sr ratio, and a variable K/Rb ratio. According to multiple techniques of dating, the metamorphic event happened between 3100 and 1200 Ma. There also are differing viewpoints on the OMTG-OMG mutual interaction. The majority of previous researchers believe the OMTG interferes with the OMG supracrustal sequence. According to later researchers, the OMG sequence was deposited on the earlier OMTG gneiss.

The three phases of the N-S elongate, oval-shaped Singhbhum granite are made up of a variety of entities. Phase 1 is a low-K granodiorite-trondhjemite, while Phases II and III are granodiorites to adamellite. Phase III is the most substantial in comparison to the previous phases. The project is divided into three phases: I, II, and III. Type A Singhbhum granite (3300-3400 Ma) is found in phases I and II, while Type B Singhbhum granite is found in phase III (3100 Ma). Singhbhum granite is a 3300-3400 Ma granodiorite-adamellite-granite suite with enclaves of OMG and OMTG (Saha, 1994). The SBG and its variants, which are assumed to have been deposited in two or three periods, dominate the Singhbhum cratonic core. The SBG massif, which is composite, comprises biotite granite, granodiorite, adamellite, and minor TTG components.

The Singhbhum Shear zone has several tiny sheets, such as lenticular bodies of granitoid. There is evidence of lit-par-lit injection of granitic material into metasediments. The succession is 2200 Ma old (Pb-Pb) (Saha, 1994).

The Bonai Granite (BG), the craton's second-largest after the SBG, covers 700 km² and is separated from the SBG by a broad swath of the western Iron Ore Belt, also known as the 10 Jamda-Koira belts (Saha, 1994). BG is mostly porphyritic and equigranular-trondhjemite-granodiorite, with some granite thrown in for good measure.

Tamperkola Granite (TG) is a minor body of granite west of the BG, separated by a band of supracrustal rocks. The TG is a K-feldspar-bearing anorogenic granite with granophyric texture. The TG has an intrusive relationship with supracrustal rocks from both the IOG and the Darjing Group, and no deformation or metamorphism characteristics are seen.

The Mayurbhanj Granite (MBG) is a batholithic mass that covers approximately 1000 km² in the south-eastern part of the Singhbhum craton, near the Singhbhum Shear Zone, and is intrusive into the SBG and the IOG (Saha, 1994). Given that it is close to the Proterozoic fold belt of North Singhbhum, the MBG is a Mesoarchean unit worried in Proterozoic deformation and metamorphism.

Some researchers interpret the SC's Archean volcano-sedimentary greenschist facies supra crustal rocks, known as the Iron Ore Group (IOG), to be truncated ophiolitic sequences and parts of the Archean oceanic crust. The relationship between the SBG and the IOG in terms of stratigraphy has long been a source of contention. The western IOG belt (Noamundi-Jamda Koira belt), the eastern IOG belt (Gorumahisani-Badampahar band), and the southern IOG belt (Tomka-Daitari belt) are the three main volcano-sedimentary supracrustal belts, commonly known as the IOG basins.

Rb-Sr dates the group between 2100 to 2300 Ma, while Pb-Pb dates it to around 3100 Ma (Saha, 1994). A lower Chaibasa Formation and an upper Dalbhum Formation make up the formation. The Dalbhum Formation is dominated by phyllites with quartzite bands and basic sills, whereas the Chaibasa Formation is dominated by garnet-staurolite-kyanite mica schists with multiple bands of quartzite, amphibolite, and acid to basic tuffs.

Green schist-amphibolite facies, phyllites, and schists border the centrally located band of the Dalma Group meta-igneous suite of rocks, forming the arcuate NSMB. The Dalma Group is made up of multiple folded greenschist- to amphibolite-facies metamorphosed mafic and ultramafic rocks with serpentinites and pillow lava horizons. To the north of the Dalma Group is the Chandil Formation, which consists of phyllite and schist interbedded with quartzite, 11 quartz-schist, graphite-phyllite, and chert.

The Newer Dolerite Dyke swarm is structured in an NW-SE, and NE-SW pattern, transgressing cratonic rocks and emplaced episodically over a long period, from Neoarchean to Paleoproterozoic.

1.3.1 Veins and Fractures

Veins are related to fracture mechanics and form when minerals are deposited by the circulation of hydrothermal fluid along fractures. Syntectonic hydrothermal quartz veins are mostly fracture-related and have a clear contact with their host rock. These hydrothermal materials fill layers, irregular and planar fractures to form shear veins and extensional veins. The outlet vein is a result of high fluid pressure (P_f) and should exceed normal compressive stress (σ_n) during the fracture (Sharma and Biswal,2019). This work focuses on paleo stress analysis the fluid pressure conditions that allowed it. mineralized flowing fluid through existing rock fracture. This work uses stereo imaging and 3D Mohr imaging. As veins and dykes are made in similar mechanism so the above process can also be used to calculate the paleo stress analysis of dykes. I have applied it to quartz and pegmatite veins of Anandpur area, North Odisha singhbhum craton, East India. These veins are extensional veins and intruded majorly into Singhbhum Granite and somewhere into gneisses. The host rock is a batholith type intrusion body which has gone under extensional setting which results in creation of fractures and then through this fracture space quartz and pegmatite veins have emplaced.

1.4 Literature review

Sarkar et al. (1977) suggested that Singhbhum shear zone (SSZ) separates a northern terrain of highly metamorphosed rocks and southern terrain of relatively less metamorphosed rocks and provided two-fold stratigraphic succession of Singhbhum dividing it into north of SSZ and south of SSZ.

Saha et al. (1994) suggested three phases of granite intrusion within Singhbhum craton based on the field relation, shapes of plutons at exposure level, primary foliation patterns, lithology and geo-chronology. These are mostly biotite rich granodiorite in composition grading to adamellite and rarely to trondhjemite.

Dey et al. (2017) studied on origin and evolution of phases of singhbhum granite and tonalite trondhjemite granodiorite (TTG).

Sharma et al. (2019) conducted paleo stress and fluid pressure analysis of vein opening from the quartz vein orientation data of Cu–Pb–Zn mineralization belt occurring in mica schist and meta-basalt of South Delhi terrane, NW India using 3D Mohr. The rock types show three prominent phases of folding, greenschist facies metamorphism and numerous phases of granitic intrusion.

Tiwari et al. (2019) used G3 granite vein's orientation of Ambaji granulite, in the South Delhi terrane of the Aravalli–Delhi mobile belt, which is intruded by four phases of granite intrusion for measurement of the paleo stress and magma pressure during its intrusion time.

Table 1 showing the stratigraphic sequence of Singhbhum Craton from Paleo Mesoarchean (after Saha 1994 and Ghosh et al., 2019)

	Major events	**Lithologies**	**Age in Ga**
		Metamorphism of OMG, OMTG, and SBG II and III	3.02-2.96
Mayurbhanj Granite and gabbro	Coeval emplacement of granite and gabbro	Granite, gabbro, anorthosite	3.09-3.08
Simlipal lava and metasediments	Formation of volcano sedimentary basin	Spilites, tuffs, quartzite	3.09
----------	Unconformity	----------	----------
SBG Type-III	Emplacement of a granitic pluton	Granodiorite to Granite	3.12
Bonai Granite		Granite to Granodiorite	3.16
Iron Ore Group	Deposition and metamorphism of Iron ore group of rocks	Mafic to felsic volcanic rocks, tuff, BIF, local dolomite, quarzitic sandstone, and conglomerate	3.3-3.1
----------	Unconformity	----------	----------
Kaptipada Granite			3.29
SBG Type II	Emplacement of granitoid plutons	Granite, tonalite and granodiorite	3.35
SBG (Singhbhum Granite) Type I	Emplacement of granitoid plutons	Tonalite, granodiorite	3.44
OMTG Granite	Intrusion of tonalitic rocks in OMG	Granite	3.32
OMTG (Older Metamorphic Tonalite Gneiss)		Tonalite gneiss and granodiorite	3.44-3.52
OMG (Older Metamorphic Group)	Deposition of sediments with volcanics	Amphibolite, pelitic schists, banded calc- gneiss	3.55-3.44
----------	Unconformity	----------	----------
Unpreserved primitive crust represented by xenocrystic zircons present in younger rocks			3.60-3.55, 3.61, 4.24-4.05

1.5 Study area

1.5.1 Location

Anandapur Tehsil is located in the south-east region of Keonjhar district, Odisha. Ghatagaon, Harichandanpur, Ghasipura, and Patna are the four blocks present in Anandapur tehsil. It has a common boundary with Mayurbhanj district along the eastern side. It is about 150 km from state capital Bhubaneswar. On the southern side of the town flows the Baitarani River. Land near the river basin is very fertile making it suitable for agriculture. Anandapur area is present within the georeferenced frame of 21.21°N, 86.11°E. The average elevation of the town is 43 m.

1.5.2 Physiography and accessibility

The study area can be approached from Keonjhar town by road through the national highway NH 20 (Keonjhar-Jamshedpur Highway) which connects Keonjhar to Anandapur. The nearest township in the area is Anandapur. The area falls under the toposheet numbers 73G/15, 73G/16, 73K/3, and 73K/4 prepared by Survey of India. The present study area is defined within the georeferenced frame of longitude E85°54'0"- E86°06'0" and latitude N21°36'0"-N21°12'0" of India. Bhandaridiha, Ghasipura, khajuripada, Sadangabahali, Ghatagaon, etc. are prominent villages in and around the study area. The Anandapur region is bordered by the Baitarani River, one of the largest rivers in the state after Mahanadi. The geomorphology of the area is characterized by uneven topography with small hills. Sendhei reserve forest, Salandi reserve forest, and Harichandanpur-Telkoi Reserve Forest are present in the surrounding area. There are a few forest ranges present nearby such as the Ghatgaon forest range, Sitabinji forest range, etc. It is a Granitic terrain. The prevailing climate is a tropical humid climate with annual rainfall of about 1550 mm. The summer months of March through June have daily high temperatures that typically exceed 40°C. In Keonjhar, May is the hottest month of the year. November to January is considered the winter months, with an average daily temperature less than 25°C. December is the coldest month of the year in Keonjhar. Vegetation is dense in the area.

1.5.3 Geology of the study area

Anandapur area is a part of central Singhbhum craton which is mostly dominated by Singhbhum Granite. Granites are occurring as large batholiths which are exhibiting weak gneissic foliations to massive in nature. Faults, joints and fractures are observed at various places indicating the area has also suffered a later brittle deformation. Along the fracture planes, intrusion of quartz veins, pegmatites, dolerite and basaltic dykes are observed. At few places within these granitic bodies, we can observe enclaves of supracrustal assemblages of Older Metamorphic Tonalite Gneiss (OMTG) which are preserved (GSI,). These rocks are showing gneissic banding. is prominent in these rocks. TTG has smoky quartz in it which gives it a dark appearance.

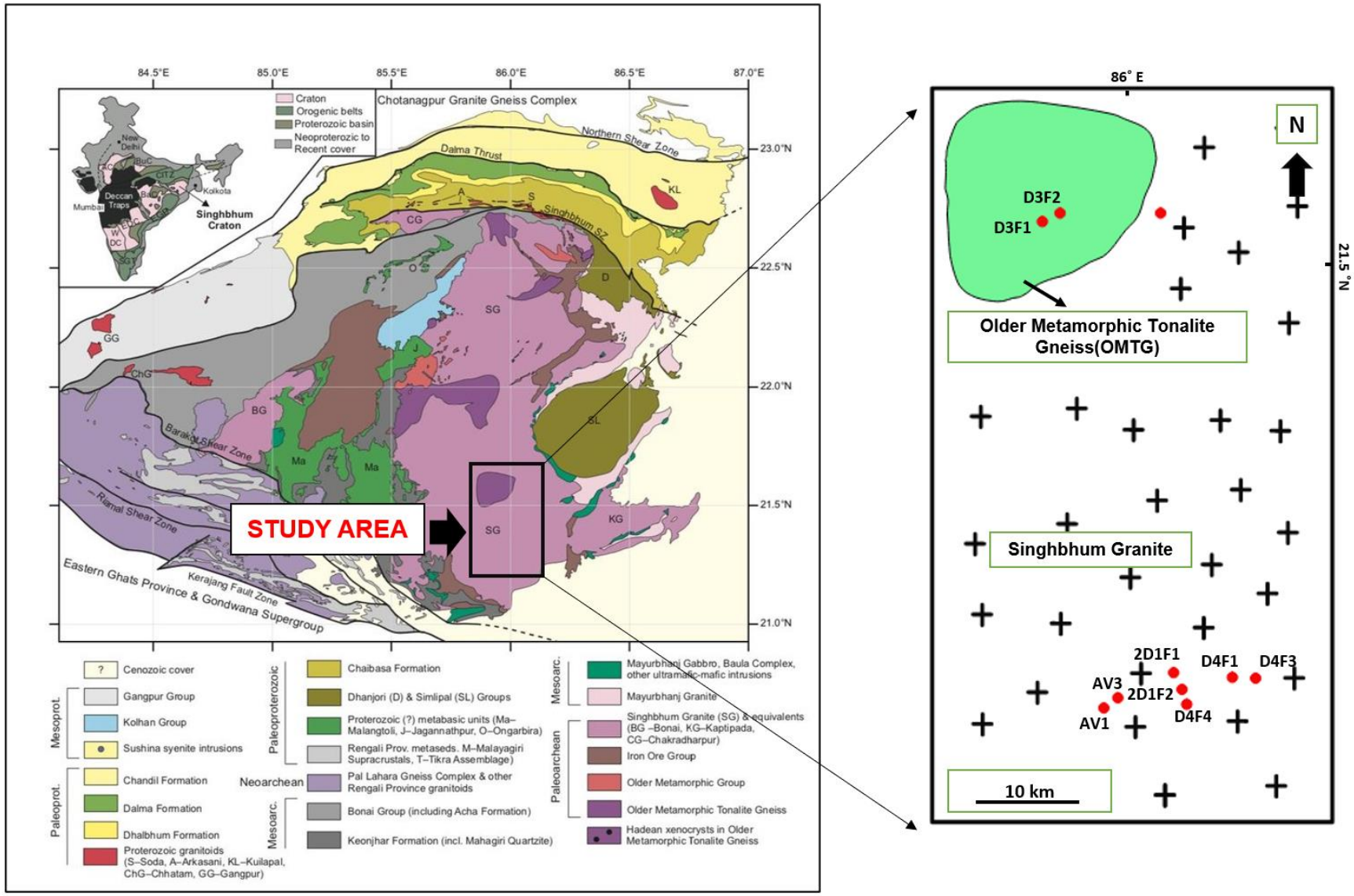

Fig 1.2: Singhbhum craton formation map showing study area and have added the placemarks in field locations using corel draw (Balushi et al., 2022).

CHAPTER 2

RESEARCH GAP AND OBJECTIVE OF STUDY

2.1 Research gap

Anandapur area is mostly dominated by granitic rocks with signatures of brittle deformation. It has numerous faults and fractures which is intruded by quartz vein, pegmatite, dolerite, basaltic dyke etc. Granite preserves the stress acting in the ancient times. Mostly study done in this area is based on petrographic, geochemical and hydrological analysis. However structural analysis and deformation structures are not well studied in this area. This area also lacks information of palaeostresses that were preexisting that led to the current deformation. Therefore, in these studies, I attempt to fulfill the existing gap regarding the palaeostress analysis of the north Singhbhum craton around the Anandapur area.

2.2 Objective

Orientation study of the veins and localized palaeostress analysis of north Odisha Singhbhum craton around Anandapur area, Keonjhar, Odisha.

CHAPTER 3

METHODOLOGY

The following methodologies have to be adopted to achieve the goal of the present study.

1. A literature review was done and toposheets along with geological maps were downloaded from the GSI site to get a preliminary idea about the study area and the topic.
2. A reconnaissance survey of the study area along with measurement of the orientation of quartz vein and fracture planes were done and few samples were collected for reference.
3. Structural and lithological field data acquisition and interpretation was done using the collected data sets.
4. Superimposition of visited locations on the formation map is done using Google Earth Pro.
5. Interpretation of lithology and regional deformation structure of the area was done using the field evidences.
6. Paleo stress analysis was performed using Stereo Net and Mohr Plotter to find out the regional stress direction and magnitude that was pre-existing in the study area.

3.1 Field data acquisition and sample collection

Instruments required:

- Working and reference map
- GPS& battery
- Clinometer and Brunton compass
- Hammer and chisel
- Hand lens
- Measuring tap
- Field notebook
- Geometric box

Before carrying out the fieldwork for the research work, proper field planning has been done. A working map of the study area was prepared. Locations with the possibility of outcrop were identified on the working map by referring to Google Earth Pro. A reconnaissance survey was carried out first to identify different rock types and deformation structures in the study area. Field scientific data of the outcrops such as lithology, structural orientations of the planar features (strike and dip), and contact nature are collected using a clinometer compass, during the fieldwork. The location (waypoints) geo coordinate, and elevation are collected by using the Global Positioning System (GPS). All the field data are geo-referenced. Rock samples collected for the petrography are also georeferenced and labeled properly with specific locations. The clinometer compass has an accuracy of 2º and GPS has a 3m accuracy.

3.2 Lithological map preparation

The base map was created using CorelDraw Software. An appropriate map of the study area is chosen and traced using this software. The traced map is georeferenced using ArcMap software. Coordinates of all the locations traversed during fieldwork are saved in Google Earth Pro software in the form of a kml file. Then these locations are transported to the traced map. All the other field information was added to the map. Legends were mentioned along with scale and coordinates.

3.3 Paleo stress analysis method

Different methods can be used to do paleo stress analysis and these are as follows-

1 – Fault-slip analysis

2- Fracture analysis

3- Numerical modelling

4 – Integrated Approach

3.3.1 Fault-Slip analysis

One of the most common methods to infer paleo stress from rock deformation is fault-slip analysis. Faults are fractures in rocks along which displacement has occurred. The direction and magnitude of the displacement indicate the orientation and intensity of the stress that caused the faulting. By measuring the orientation, slip direction, and

slip sense of multiple faults in a region, you can construct a stress tensor that represents the principal stress axes and their magnitudes at the time of faulting. This stress tensor can then be used to classify the type of faulting (e.g., normal, reverse, strike-slip, or oblique) and the tectonic regime (e.g., extensional, compressional, or transcurrent) that prevailed in the past.

3.3.2 Fractures and Veins analysis

Fracture analysis is an additional method for estimating paleo stress from rock deformation. Fractures are cracks in rocks that have not moved significantly. They occur when the stress exceeds the strength of the rock, causing tensile or shear damage. By measuring the direction, distance, length, and opening of fractures, you can determine the direction and magnitude of the stress that caused the fracture. In addition, rock strain rate, fluid pressure, and heat history can all be deduced from the fracture analysis method. For example, fractures filled with minerals or fluids indicate that the rock was permeable and fluid circulation occurred after the fracture. Curved or cross-sectional fractures of other fractures indicate that the rock has undergone several cycles of deformation or rotation.

3.3.3 Numerical modeling

Numerical modeling is another way to derive paleo stress and paleo strain from rock deformation. The application of mathematical formulas and computer simulations to simulate and predict rock behavior under various stress and strain scenarios is called numerical modeling. By inputting the physical properties, boundary conditions, and initial conditions of the rock system, a numerical model can be created that can reproduce observed deformation characteristics or predict possible deformation scenarios. In addition to exploring parameter sensitivities and uncertainties and underlying assumptions, numerical modeling can also be used to test and confirm results from other techniques.

3.3.4 Integrated approach

An integrated approach is another technique for determining paleo stress and paleo strain from rock deformation. Combining several techniques and data sources results in an integrated approach that provides a more thorough and trustworthy analysis of the deformation history. You can get around the drawbacks and uncertainties of each

method and cross-check and validate the outcomes by integrating other methods and data. To constrain the paleo stress field, for instance, you can use fault-slip analysis and fracture analysis; to constrain the paleo strain field, you can use strain marker analysis and fabric analysis; and to simulate and validate the deformation process, you can use numerical modeling.

From the above methods for paleo stress analysis, I have chosen the 2nd method which is fractures and veins analysis method which is discussed in detail in the following paragraph.

Quartz vein orientation and fracture data taken from the field are plotted in equal area net through **Stereonet** software and a 3D Mohr circle is also constructed. The dip amount and dip direction of Quartz vein orientation and fracture plane data which are collected from the field are arranged in a table. Then they are plotted in stereonet software. Poles of the fracture planes are plotted. Then contouring of the pole data is done which indicates the pole density. Maximum concentration is observed in the N-W quadrant and two sub-maximum concentrations are observed in the south-western quadrant. Then a best-fit ellipse is made using CorelDRAW in the area and the ellipse is rotated and aligned to a north-south position. Then the major axis and the minor axis are aligned to a suitable great circle and then the ellipse is brought back to its original position. We have two great circles aligned to the major and minor axis of the ellipse. The center of the ellipse is considered as σ_1. The fracture plane is formed at 30° to σ_1 which means it is at 60° to the pole of the fracture plane. So σ_1 is the obtuse bisectrix of the pole of two fracture planes created. So, we take the region with no pole density for drawing a best-fit ellipse whose center can act as σ_1. σ_3 will be the acute bisectrix for the poles of the fracture planes. So, the region with highethe st pole density is considered for plotting σ_3. σ_2 is perpendicular to the minor axis which is located along the major-axis. Then the σ_1, σ_2 and σ_3 values are plotted in the 3D Mohr circle to obtain the stress ellipsoid. From it the orientation and magnitudes of planes in a rock, normal and shear stresses can be analysed. relationship between rock strength and state of stress under which the rock fractures can be predicted from it.

3.4 Theoretical Concept

3.4.1 Fracture Opening Conditions

The fluid pressure needs to be higher than the normal stress (σ_n) acting on the fracture wall in order to open the pre-existing fracture (fig 3.1) (Delaney et al., 1986):

$$P_f \geq \sigma_n, \quad (1)$$

Where P_f = Pore fluid pressure and σ_n = Normal stress

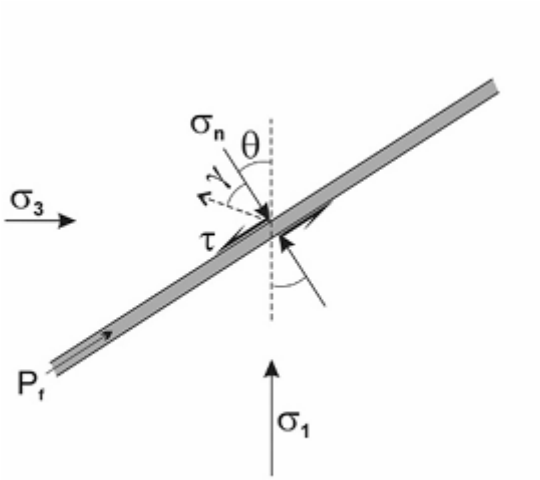

Fig 3.1: Diagrammatic two-dimensional illustration of a planar discontinuity opening with normal stress on its walls exceeded by pore fluid pressure (P_f) at a certain

The angle γ is the direction of opening and θ is the angle between maximum principal stress (σ_1) and normal principal stress (σ_n).

The stress on the fracture plane must be in the shaded region of (Fig. 2) in order for this requirement to be satisfied. The Normal stress (σ_n) acting on the fracture plane (fig 3.1) can be deduced from the θ and maximum principal stress (σ_1) and minimum principal stress (σ_3) (Jolly and Sanderson, 1997) by applying following equation,

$$\sigma_n = \frac{\sigma_1+\sigma_3}{2} + \frac{\sigma_1-\sigma_3}{2} \cos 2\theta \quad (2)$$

Delaney et al. (1986) derived the driving stress ratio (R) by putting and rearranging the value of equation (2) in equation (1):

$$R = \frac{P_f - \frac{\sigma_1 + \sigma_3}{2}}{\frac{\sigma_1 - \sigma_3}{2}} \geq cos\, 2\theta \quad (3)$$

This can also be expressed in terms of the maximum shear (τ max) stress and the mean stress (σ_m) (Jolly and Sanderson, 1997)

$$R = \frac{P_f - \sigma_m}{\tau_{max}} \geq cos\, 2\theta \quad (4)$$

Delaney et al. (1986) referred to parameter R as the driving stress ratio, which shows how fluid pressure, the maximum shear (τ max) stress and the mean stress (σ_m) affects fracture opening conditions.

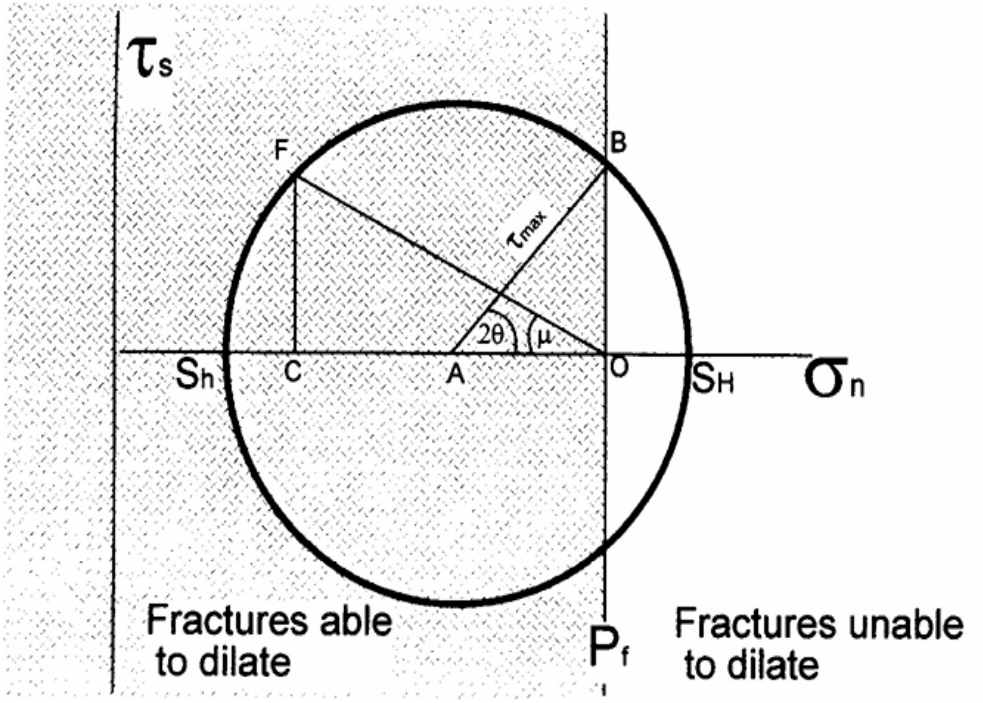

Fig 3.2: The maximum principal stress (σ_n), maximum shear stress (τ_{max}), and minimum principal stress (σ_3), are displayed on a Mohr circle construction. Plotting the fluid pressure (P_f) along the normal stress (σ_n) axis is done. Because the usual stress is lower than the fluid pressure, fractures in the shaded area to the left of the fluid pressure line can enlarge. It is not possible for fractures to enlarge to the right of the fluid pressure line. The triangle FOC determines the opening direction (μ) of a fracture, and the triangle AOB is utilized to calculate the R ratio (Jolly and Sanderson, 1997).

The ability of fractures to dilate is determined by the fluid pressure position in the two-dimensional Mohr circle. The fracture will enlarge if Pf ≥ σn, and vice versa. The range of fracture orientations that will open in a specific stress condition is provided by this construction (Sharma and Biswal, 2019).

3.4.2 3D Mohr Circle Construction

In order to open pre-existing fractures and measure relative stress, the 3D Mohr circle construction was developed. The fluid condition is calculated using the pole-to-vein pattern. The creation of a 3D Mohr circle takes into account the maximum (σ_1), intermediate (σ_2), and minimum (σ_3) principal stress, with compression always being regarded as positive.

Three circles make up the 3D Mohr diagram; these circles represent the σ_1–σ_2, σ_1–σ_3, and σ_2–σ_3 planes. In order to characterize the state of stress and fluid pressure, two new terms were introduced: the driving pressure ratio (R) which characterizes the difference between the principal stress axes and the condition of fluid pressure and the stress ratio (ϕ), which defines the shape of the stress ellipsoid and describes the relative magnitude of the principal stress axes by characterizing σ_2 in relation to σ_1 and σ_3 (Sharma and Biswal, 2019).

$$\phi = \frac{\sigma_2 - \sigma_3}{\sigma_1 - \sigma_3} = \frac{1 + cos\, 2\theta_2}{1 + cos\, 2\theta_1}$$

$$= 1 - \frac{1 - cos\, 2\theta_2}{1 - cos\, 2\theta_3} \quad (5)$$

$$R' = \frac{P_f - \sigma_3}{\sigma_1 - \sigma_3} = \frac{1 + cos\, 2\theta_2}{2} \quad (6)$$

The value of stress ratio (ϕ) varies from 0 to 1; the lower value of ϕ denotes a prolate stress ellipsoid, where the magnitude of σ_2 is closer towards the σ_3 than σ_1 and the stress ratio will increase when the magnitude of σ_2 will move from σ_3 towards σ_1 along the normal stress axis in Mohr circle which results in oblate stress ellipsoid (Sharma and Biswal, 2019)

The value of driving pressure ratio (R') also varies from 0 to 1 (0<R'<1). From equation (6), when R' = 0, the magnitude of pore fluid pressure (P_f) is same with the magnitude of σ_3 ($P_f = \sigma_3$) and when R' = 1, the magnitude of pore fluid pressure (P_f) is same with the magnitude of σ_1 ($P_f = \sigma_1$). The difference between R ratio and R' of Delaney et al. (1986) is, the driving pressure ratio R is expressed in terms of P_f and σ_m, whereas the R' is expressed in terms of P_f and σ_3 (Sharma and Biswal, 2019).

By using the stereographic projection of fractures and veins data and their distribution data the driving pressure and relative stress are determined and by constructing 3D Mohr circle using these data the condition of fluid pressure can be defined. Using the stereographic projection of data, measure 2θ (twice the angle between normal stress (pole to vein) and the maximum principal stress direction), where θ indicates the orientation of fractures that can widen under conditions of high fluid pressure. In the $\sigma_2 - \sigma_3$, $\sigma_1 - \sigma_3$, and $\sigma_1 - \sigma_2$ planes, angles θ_1, θ_2, and θ_3 are therefore measured. In the case where $P_f > \sigma_2$, the poles to vein form a girdle type distribution perpendicular to σ_1, while in the case where $P_f < \sigma_2$, the poles to vein define a cluster type distribution around σ_3. The σ_1 is located in the middle of the vacant elliptical region in the stereonet's girdle distribution of the pole to vein. This makes it easier in measuring the angles θ_2 and θ_3 of the planes as well as the σ_1–σ_3 and σ_1–σ_2 planes. (Sharma and Biswal, 2019).

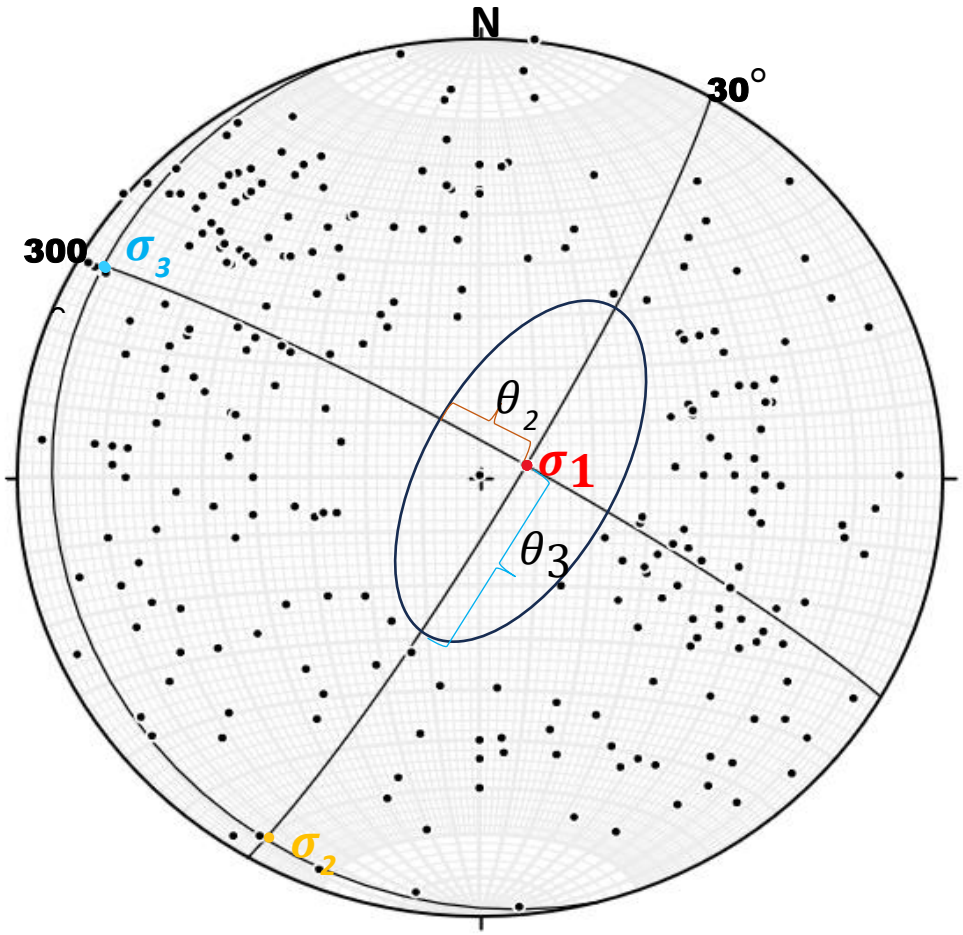

Fig 3.3: orientation of σ1, σ2, and σ3 as determined from the quartz vein's girdle distribution, while θ2 and θ3 are determined from the ellipse

CHAPTER 4

STRUCTURAL ANALYSIS

4.1 Fieldwork

Field studies and laboratory studies can be used to categorize the geological investigations. In geology, experiments are not at all feasible. (N.W. Gokhale, 2015) For example, in no laboratory is it possible to prepare rocks, on the scale, as are found in the crust of the earth. The majority of the geological research are identification-based; whether of a rock, a mineral, a fault, or a fossil, and so on. The primary goal of the field investigations is, in the end, to map out the geological distribution of the rocks as well as structural characteristics like faults and folds. Only if the field studies are conducted then the laboratory work can be carried out like microscopic and megascopic identifications, and chemical analysis of rock samples. The purpose of the laboratory research is to support the findings of the field studies, not the other way around. Therefore, field studies play a big role in Geological Investigations. In this instance, fieldwork is very essential for the completion of the project work. It required detailed fieldwork to collect all the data of the lithological variation, exposures present within the study area, structures and microstructures exposed, and planar and linear data of bedding planes, which has taken a long time and is a major part of the project. So detailed fieldwork has been done in the study area, a large area has been covered for reconnaissance survey and finding out the exposures. The lithological survey has been done; several structural data has been collected at the exposures.

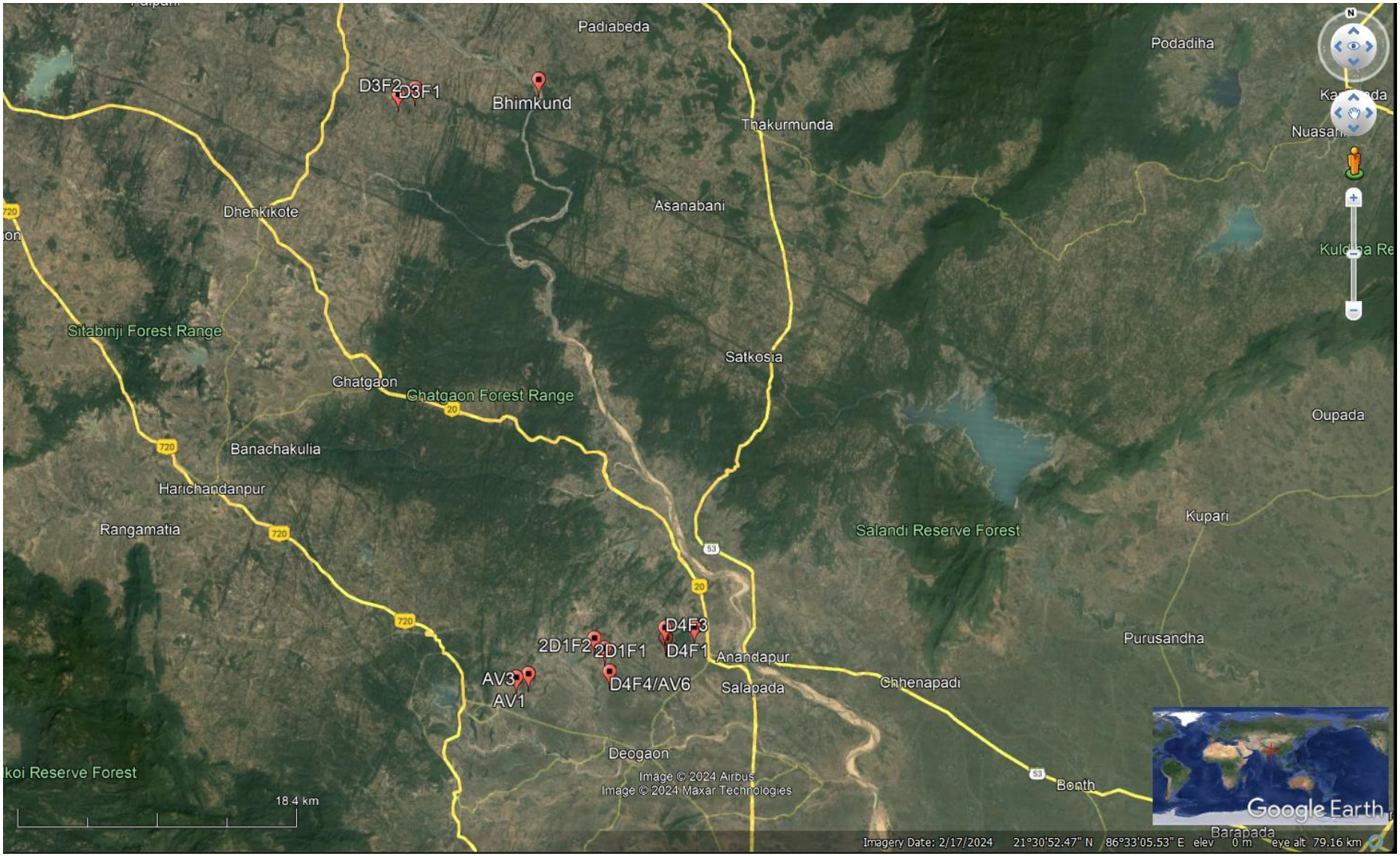

Fig 4.1: Satellite image of locations visited

Location 1- 21°12’02” N

(AV1) **85°58’26” E**

Elevation - **326 m**

These locations are dominated by granitic batholiths with intrusion of quartz veins. Granitic terrain has undergone spheroidal weathering. It is a type of chemical weathering that affects mostly jointed bedrocks. Pegmatite veins having around 20 cm width are intruded there in conjugate manner. Quartz and feldspar are the common minerals that can be spotted with naked eye having diameter around 0.5 cm. Feldspar is exhibiting 2 sets of cleavage. Three sets of joints can be clearly seen (fig 4.2).

Location 2 - 21°13'18"N

(2D2F1) **86°01'24"E**

Elevation – 110m

These locations are also dominated by granitic rocks with intrusion of quartz veins. The contact in between granitic rocks and quartz veins are gradational type which indicates slow intrusion by reacting with the granitic host rock and in this location, I found plagioclase feldspar clearly showing 2 sets of cleavage (fig 4.3).

Location 3 - 21°33'07"N

(Bhimkund) **86°01'01"E**

Elevation – 288m

This location is in Bhimkund, Keonjhar region where a big mafic dyke intruded into the well foliated gneissic rock, where the contact in between the host and the mafic dyke is sharp which can be clearly seen in google earth pro as well. This region has also undergone into intense stress condition which results in creating fracture planes with average spacing around 5 cm. Some of these fracture planes are intruded by pegmatites and quartz veins (fig 4.4).

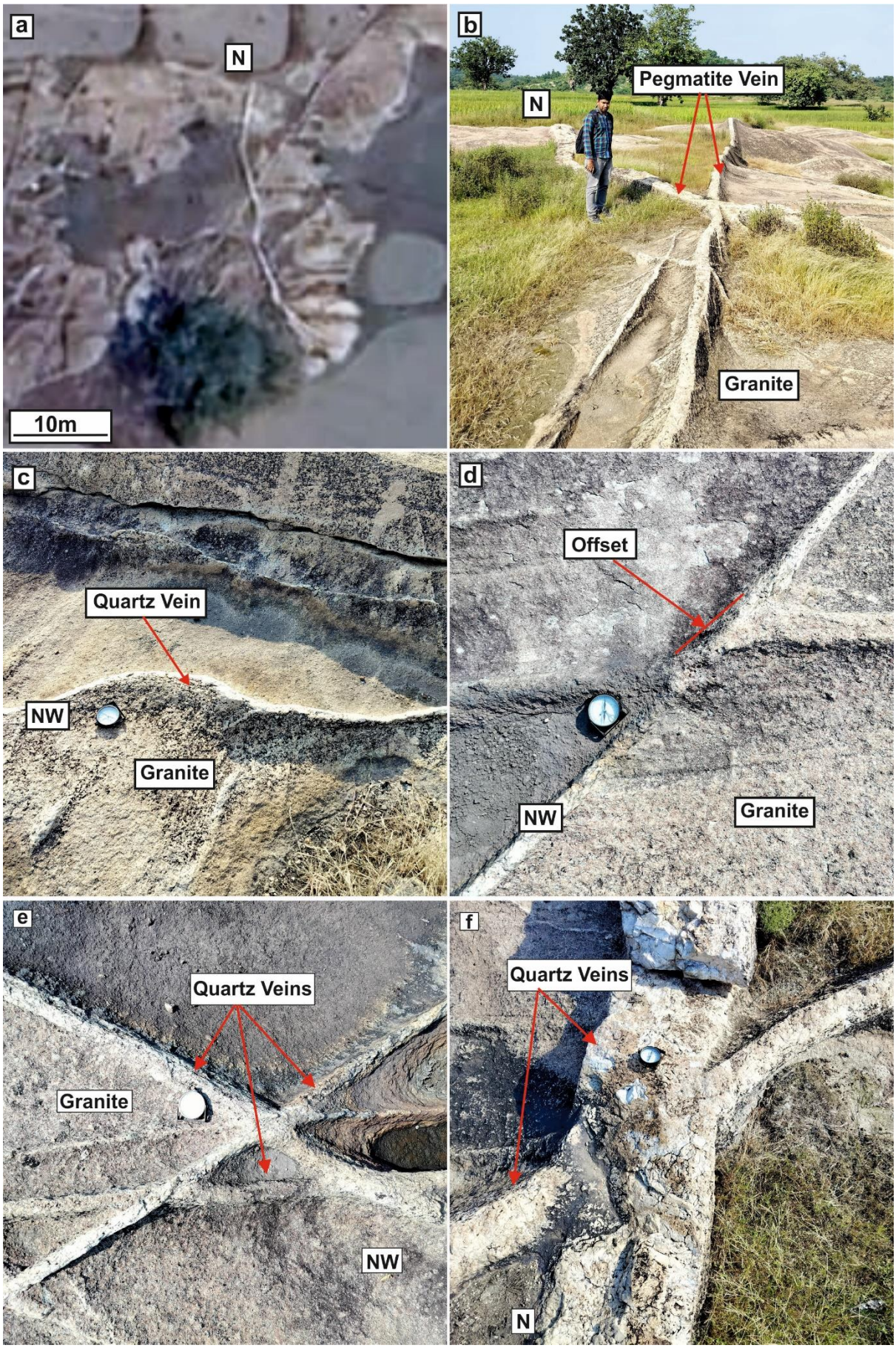
a
N
10m
b
Pegmatite Vein
N
Granite
c
Quartz Vein
NW
Granite
d
Offset
NW
Granite
e
Quartz Veins
Granite
NW
f
Quartz Veins
N

Fig 4.2: Field photographs of Quartz vein in Singhbhum granite of Anandpur region is showing extensional veins (a) Pegmatite veins clearly visible on google earth pro satellite image orienting N-S (b) In the image, the first phase of the N-S oriented plagioclase-rich pegmatite vein intersects with the later phase of the NE-SW oriented pegmatite vein. (c) NW-SE oriented curved quartz vein in exfoliated granite (d) The first phase of NW-SE oriented quartz vein is intersecting the later phase of N-S oriented quartz vein which created an offset in the first phase quartz vein (e) Three sets of orienting NW-SE, NE-SW and E-W are intersecting each other in granite hosted rock (f) NE-SW oriented quartz vein is intersects with the later phase of N-S oriented pegmatite veins

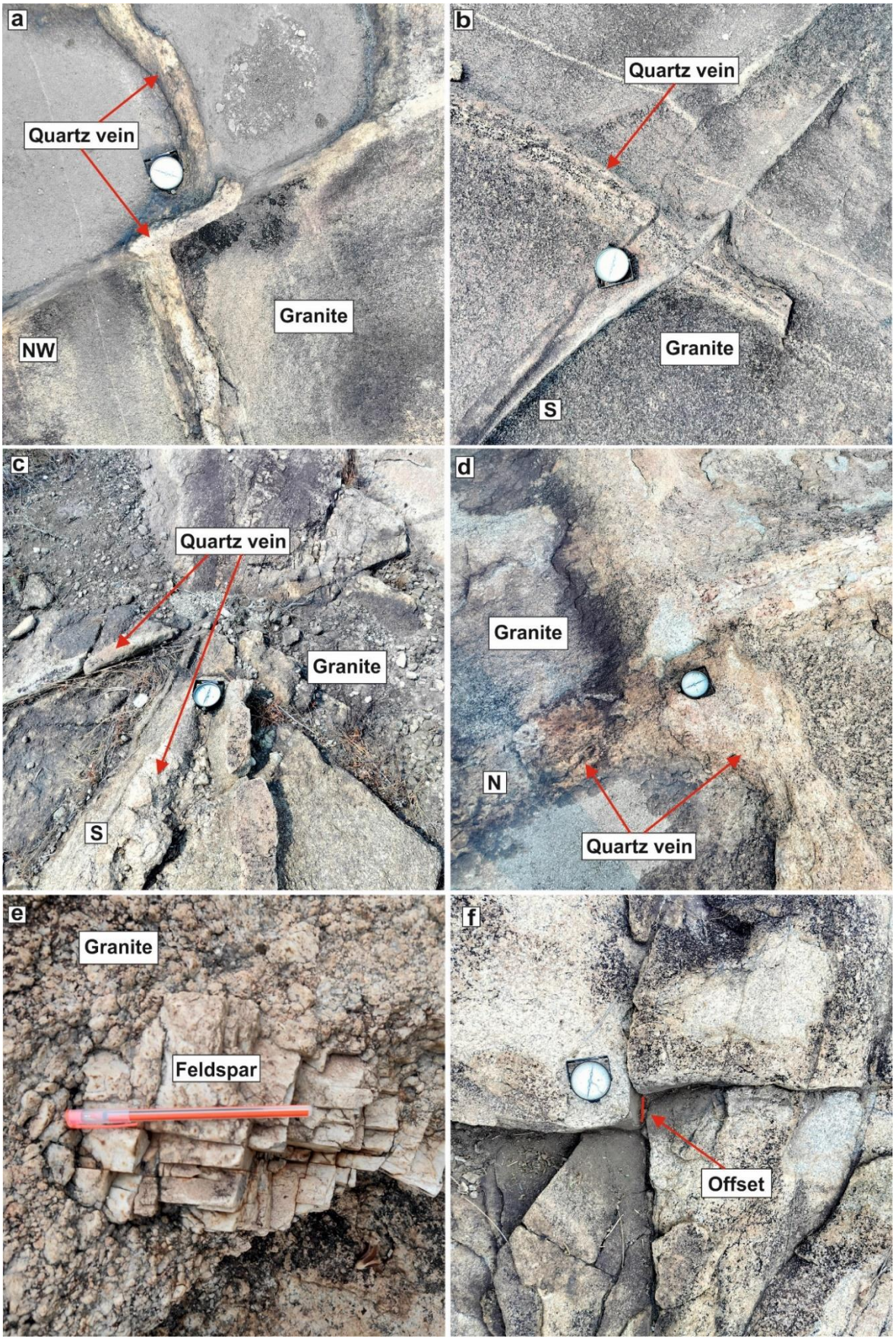
a
Quartz vein
Granite
NW
b
Quartz vein
Granite
S
c
Quartz vein
Granite
S
d
Granite
N
Quartz vein
e
Granite
Feldspar
f
Offset

Fig 4.3: (a) In the image, the first phase of the NE-SW oriented quartz vein intersects with the later phase of the NW-SE oriented quartz vein. (b) Quartz vein in granitic hosted rock showing gradational contact with the host rock. (c) Three sets of quartz veins orienting N-S, NE-SW and NW-SE are intersecting each other at a common point. (d) Conjugate sets of quartz veins orienting N-S and E-W are intersecting each other and showing some degree of offset. (e) Feldspar clearly showing 2 sets of cleavage. (f) Two sets of conjugate fracture planes orienting N-S and E-W are intersecting each other and showing offsets.

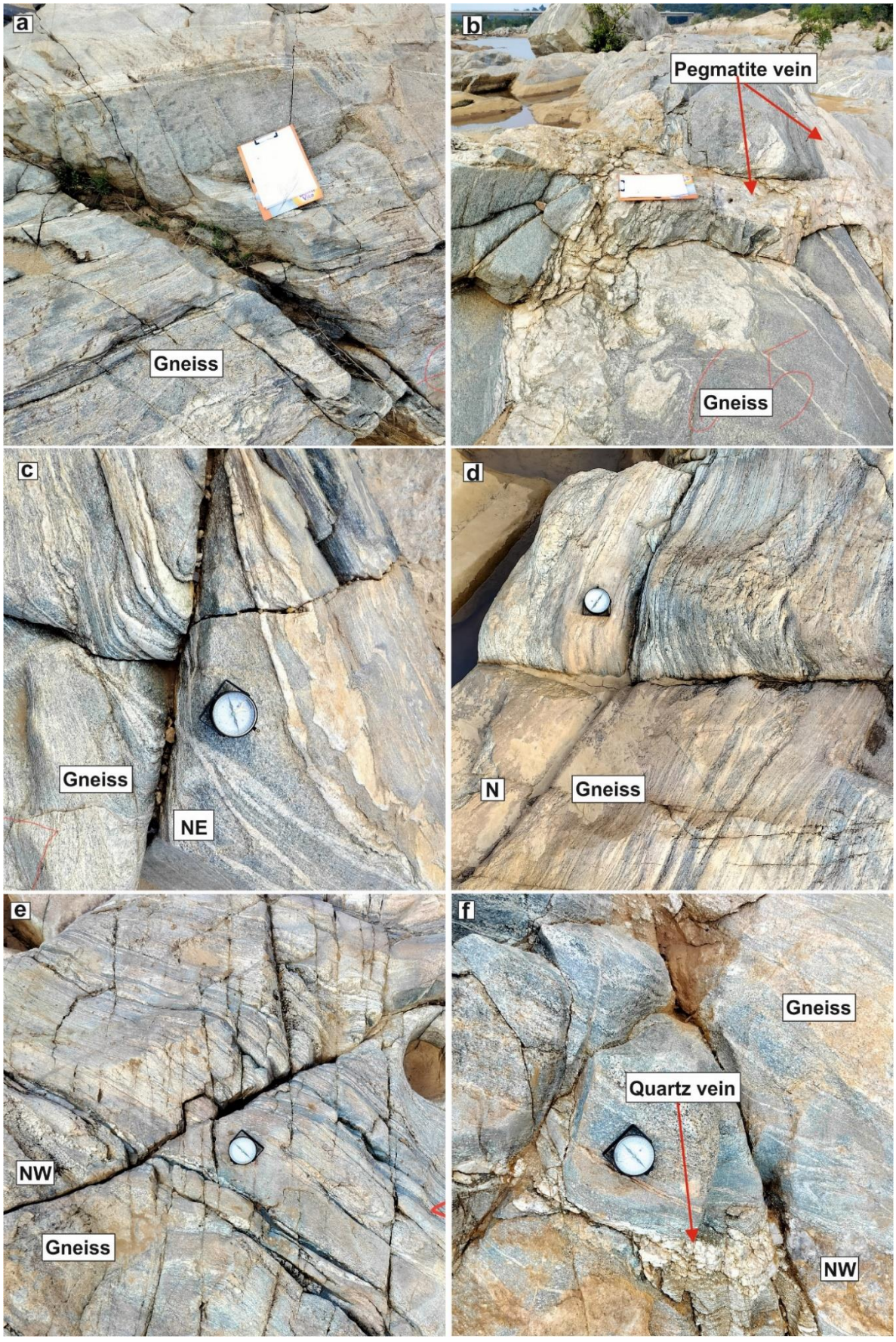
a
Gneiss
b
Pegmatite vein
Gneiss
c
Gneiss
NE
d
N
Gneiss
e
NW
Gneiss
f
Gneiss
Quartz vein
NW

Fig 4.4: Intense brittle deformation has occurred in this area (a) A fracture having space around 15 cm is conjugately intersecting with another fracture having space around 5 cm. (b) Two conjugate pegmatite veins are intersecting each other having thickness around 15 cm. (c) The early phase SE-NW oriented fracture plane is intersecting the later phase of NE-SW oriented fracture plane and offset has formed. (d) The N-S oriented fracture plane is intersecting with the E-W oriented fracture plane and offset has formed in well foliated gneissic host rock. (e) Three sets of fracture planes are intersecting each other and resulting a triangular shape structure in gneissic host rock. (f) A quartz vein orienting NW-SE intersecting with NE-SW fracture plane.

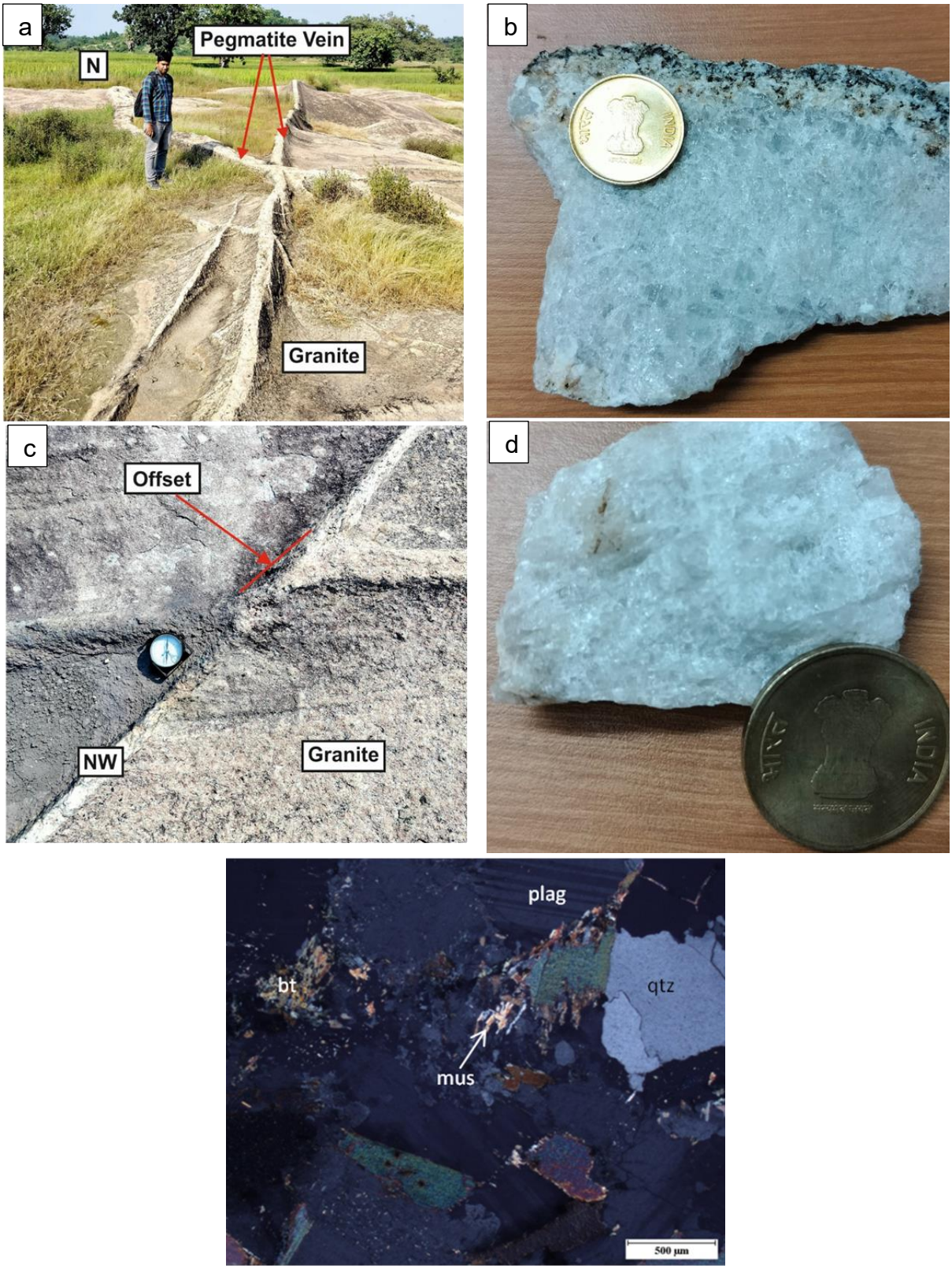

Fig 4.5: Megascopic and thin section study (a) Showing N-S and NE-SW oriented pegmatitic veins (b) Sample taken from pegmatitic vein in (a) and showing big grains of plg and feldspar (c) Conjugate quartz veins (d) sample taken from quartz vein in (c) showing big grains of qtz (e) Showing thin section of host granite rock.

Table 2

Sl No.	Location	Dip amount (in degree)	Dip direction (in degree)	Thickness of Fracture (in cm)
1	21° 12' 3.78" N 85° 58' 25.536" E	56	295	12
2	21° 12' 3.78" N 85° 58' 25.536" E	40	27	4.5
3	21° 12' 3.78" N 85° 58' 25.536" E	46	200	2
4	21° 12' 3.78" N 85° 58' 25.536" E	55	345	4
5	21° 12' 3.78" N 85° 58' 25.536" E	50	310	3.5
6	21° 12' 3.78" N 85° 58' 25.536" E	50	308	5
7	21° 12' 3.78" N 85° 58' 25.536" E	62	245	6
8	21° 12' 3.78" N 85° 58' 25.536" E	50	34	3
9	21° 12' 3.78" N 85° 58' 25.536" E	53	355	8
10	21° 12' 3.78" N 85° 58' 25.536" E	50	321	4
11	21° 12' 3.78" N 85° 58' 25.536" E	25	297	5
12	21° 12' 3.78" N 85° 58' 25.536" E	45	140	2
13	21° 12' 3.78" N 85° 58' 25.536" E	70	8	8
14	21° 12' 3.78" N 85° 58' 25.536" E	60	14	5
15	21° 12' 3.78" N 85° 58' 25.536" E	52	145	5
16	21° 12' 3.78" N 85° 58' 25.536" E	40	90	43
17	21° 12' 3.78" N 85° 58' 25.536" E	70	305	4
18	21° 12' 3.78" N 85° 58' 25.536" E	50	12	6
19	21° 12' 3.78" N 85° 58' 25.536" E	40	10	16
20	21° 12' 3.78" N 85° 58' 25.536" E	70	140	6
21	21° 12' 3.78" N 85° 58' 25.536" E	80	154	3.5
22	21° 12' 3.78" N 85° 58' 25.536" E	62	135	3
23	21° 12' 3.78" N 85° 58' 25.536" E	75	340	8
24	21° 12' 3.78" N 85° 58' 25.536" E	26	75	3
25	21° 12' 3.78" N 85° 58' 25.536" E	50	130	2.5
26	21° 12' 3.78" N 85° 58' 25.536" E	80	270	3.5
27	21° 12' 3.78" N 85° 58' 25.536" E	60	220	30
28	21° 12' 3.78" N 85° 58' 25.536" E	55	272	50
29	21° 12' 3.78" N 85° 58' 25.536" E	65	133	18
30	21° 12' 3.78" N 85° 58' 25.536" E	65	134	5
31	21° 12' 3.78" N 85° 58' 25.536" E	52	108	12
32	21° 12' 3.78" N 85° 58' 25.536" E	50	345	6
33	21° 12' 3.78" N 85° 58' 25.536" E	70	135	5.5
34	21° 12' 3.78" N 85° 58' 25.536" E	30	287	3
35	21° 12' 3.78" N 85° 58' 25.536" E	40	355	3
36	21° 12' 3.78" N 85° 58' 25.536" E	45	342	7
37	21° 12' 3.78" N 85° 58' 25.536" E	65	75	2.5
38	21° 33' 0.396" N 85° 55' 40.728" E	80	15	3
39	21° 33' 0.396" N 85° 55' 40.728" E	75	320	4.2
40	21° 33' 0.396" N 85° 55' 40.728" E	83	150	4.5
41	21° 33' 0.396" N 85° 55' 40.728" E	80	300	3.5
42	21° 33' 0.396" N 85° 55' 40.728" E	30	185	4
43	21° 33' 0.396" N 85° 55' 40.728" E	40	262	2

44	21° 33' 0.396" N 85° 55' 40.728" E	75	300	5
Sl No.	Location	Dip amount (in degree)	Dip direction (in degree)	Thickness of Fracture (in cm)
45	21° 33' 0.396" N 85° 55' 40.728" E	33	195	3.5
46	21° 33' 0.396" N 85° 55' 40.728" E	75	262	4
47	21° 33' 0.396" N 85° 55' 40.728" E	80	22	7
48	21° 33' 0.396" N 85° 55' 40.728" E	43	277	6
49	21° 33' 0.396" N 85° 55' 40.728" E	72	195	3
50	21° 33' 0.396" N 85° 55' 40.728" E	13	205	3
51	21° 33' 0.396" N 85° 55' 40.728" E	70	20	5
52	21° 33' 0.396" N 85° 55' 40.728" E	80	127	4
53	21° 33' 13.212" N 85° 56' 19.212" E	21	10	8
54	21° 33' 13.212" N 85° 56' 19.212" E	85	180	7
55	21° 33' 13.212" N 85° 56' 19.212" E	80	125	5
56	21° 33' 13.212" N 85° 56' 19.212" E	43	112	6
57	21° 33' 7.38" N 86° 1' 1.416" E	46	133	5
58	21° 33' 7.38" N 86° 1' 1.416" E	35	235	5
59	21° 33' 7.38" N 86° 1' 1.416" E	75	160	7
60	21° 33' 7.38" N 86° 1' 1.416" E	25	245	7
61	21° 33' 7.38" N 86° 1' 1.416" E	56	305	5
62	21° 33' 7.38" N 86° 1' 1.416" E	75	195	4.5
63	21° 33' 7.38" N 86° 1' 1.416" E	85	340	3.5
64	21° 33' 7.38" N 86° 1' 1.416" E	75	312	19
65	21° 33' 7.38" N 86° 1' 1.416" E	40	250	2
66	21° 33' 7.38" N 86° 1' 1.416" E	30	25	70
67	21° 33' 7.056" N 86° 1' 2.316" E	40	250	18
68	21° 33' 7.056" N 86° 1' 2.316" E	85	302	2
69	21° 33' 7.056" N 86° 1' 2.316" E	71	215	1
70	21° 33' 7.056" N 86° 1' 2.316" E	85	315	0.5
71	21° 33' 7.056" N 86° 1' 2.316" E	45	175	2
72	21° 33' 7.056" N 86° 1' 2.316" E	45	250	3
73	21° 33' 7.056" N 86° 1' 2.316" E	62	332	1
74	21° 33' 7.056" N 86° 1' 2.316" E	42	192	1.5
75	21° 33' 7.056" N 86° 1' 2.316" E	50	242	2
76	21° 33' 7.056" N 86° 1' 2.316" E	75	325	1
77	21° 33' 7.056" N 86° 1' 2.316" E	90	187	0.5
78	21° 33' 7.056" N 86° 1' 2.316" E	82	323	1.2
79	21° 33' 7.056" N 86° 1' 2.316" E	70	322	7.2
80	21° 33' 7.056" N 86° 1' 2.316" E	57	251	7
81	21° 33' 7.056" N 86° 1' 2.316" E	85	8	1
82	21° 33' 7.056" N 86° 1' 2.316" E	40	253	3
83	21° 33' 7.056" N 86° 1' 2.316" E	61	132	0.8
84	21° 33' 7.056" N 86° 1' 2.316" E	34	313	2
85	21° 33' 7.056" N 86° 1' 2.316" E	85	147	5
86	21° 33' 7.056" N 86° 1' 2.316" E	45	233	0.7
87	21° 33' 7.056" N 86° 1' 2.316" E	74	150	1
88	21° 33' 7.056" N 86° 1' 2.316" E	85	21	1

Sl No.	Location	Dip amount (in degree)	Dip direction (in degree)	Thickness of Fracture (in cm)
89	21° 33' 7.056" N 86° 1' 2.316" E	76	137	3
90	21° 33' 7.056" N 86° 1' 2.316" E	75	235	3.5
91	21° 33' 7.056" N 86° 1' 2.316" E	75	140	1
92	21° 33' 7.056" N 86° 1' 2.316" E	45	265	1
93	21° 33' 7.056" N 86° 1' 2.316" E	82	134	1.2
94	21° 33' 7.056" N 86° 1' 2.316" E	87	133	3
95	21° 33' 7.056" N 86° 1' 2.316" E	85	137	1.4
96	21° 33' 7.056" N 86° 1' 2.316" E	87	33	2.3
97	21° 33' 7.056" N 86° 1' 2.316" E	80	53	1
98	21° 33' 7.056" N 86° 1' 2.316" E	51	237	4
99	21° 33' 7.056" N 86° 1' 2.316" E	48	168	0.8
100	21° 33' 7.056" N 86° 1' 2.316" E	69	152	0.5
101	21° 33' 7.056" N 86° 1' 2.316" E	70	43	0.4
102	21° 33' 7.056" N 86° 1' 2.316" E	90	130	0.5
103	21° 13' 24.204" N 86° 5' 13.704" E	50	177	1.5
104	21° 13' 24.204" N 86° 5' 13.704" E	50	53	1.5
105	21° 13' 24.204" N 86° 5' 13.704" E	35	150	2.5
106	21° 13' 24.204" N 86° 5' 13.704" E	42	260	5
107	21° 13' 6.132" N 86° 4' 7.464" E	75	130	3
108	21° 13' 6.132" N 86° 4' 7.464" E	68	92	4
109	21° 13' 6.132" N 86° 4' 7.464" E	60	302	8
110	21° 13' 6.132" N 86° 4' 7.464" E	36	252	2
111	21° 13' 6.132" N 86° 4' 7.464" E	60	117	5
112	21° 13' 6.132" N 86° 4' 7.464" E	60	180	6
113	21° 13' 6.132" N 86° 4' 7.464" E	48	83	4.5
114	21° 13' 6.132" N 86° 4' 7.464" E	35	202	2.6
115	21° 13' 6.132" N 86° 4' 7.464" E	55	87	2
116	21° 13' 6.132" N 86° 4' 7.464" E	35	131	13
117	21° 13' 6.132" N 86° 4' 7.464" E	25	175	17
119	21° 13' 6.132" N 86° 4' 7.464" E	45	325	17
120	21° 13' 6.132" N 86° 4' 7.464" E	45	222	12
121	21° 13' 6.132" N 86° 4' 7.464" E	48	120	11
122	21° 13' 6.132" N 86° 4' 7.464" E	62	335	3.5
123	21° 13' 6.132" N 86° 4' 7.464" E	52	280	2
124	21° 13' 6.132" N 86° 4' 7.464" E	70	72	2
125	21° 13' 6.132" N 86° 4' 7.464" E	40	290	2
126	21° 13' 6.132" N 86° 4' 7.464" E	55	255	4
127	21° 13' 6.132" N 86° 4' 7.464" E	52	123	3
128	21° 13' 6.132" N 86° 4' 7.464" E	55	32	2.5
129	21° 13' 6.132" N 86° 4' 7.464" E	35	175	0.5
130	21° 13' 6.132" N 86° 4' 7.464" E	75	275	18
131	21° 13' 6.132" N 86° 4' 7.464" E	70	65	6
132	21° 13' 6.132" N 86° 4' 7.464" E	41	80	2
133	21° 13' 6.132" N 86° 4' 7.464" E	62	200	4
134	21° 13' 6.132" N 86° 4' 7.464" E	43	125	23

Sl No.	Location	Dip amount (in degree)	Dip direction (in degree)	Thickness of Fracture (in cm)
135	21° 13' 6.132" N 86° 4' 7.464" E	48	236	3.5
136	21° 13' 6.132" N 86° 4' 7.464" E	50	242	3
137	21° 13' 6.132" N 86° 4' 7.464" E	75	242	23
138	21° 13' 6.132" N 86° 4' 7.464" E	32	150	3.7
139	21° 13' 6.132" N 86° 4' 7.464" E	40	252	5
140	21° 13' 6.132" N 86° 4' 7.464" E	30	285	1.5
141	21° 13' 6.132" N 86° 4' 7.464" E	50	335	1.5
142	21° 13' 6.132" N 86° 4' 7.464" E	87	170	19
143	21° 13' 6.132" N 86° 4' 7.464" E	34	313	5
144	21° 13' 6.132" N 86° 4' 7.464" E	52	260	3
145	21° 13' 6.132" N 86° 4' 7.464" E	50	262	15
146	21° 13' 6.132" N 86° 4' 7.464" E	67	120	2
147	21° 13' 6.132" N 86° 4' 7.464" E	74	282	10
148	21° 13' 6.132" N 86° 4' 7.464" E	55	150	25
149	21° 13' 6.132" N 86° 4' 7.464" E	65	292	6
150	21° 13' 6.132" N 86° 4' 7.464" E	55	155	6.2
151	21° 13' 6.132" N 86° 4' 7.464" E	42	100	1.2
152	21° 13' 6.132" N 86° 4' 7.464" E	32	140	11
153	21° 13' 6.132" N 86° 4' 7.464" E	80	248	16
154	21° 13' 6.132" N 86° 4' 7.464" E	66	175	15.5
155	21° 13' 6.132" N 86° 4' 7.464" E	26	186	8
156	21° 13' 6.132" N 86° 4' 7.464" E	70	55	7
157	21° 13' 6.132" N 86° 4' 7.464" E	82	186	13
158	21° 13' 6.132" N 86° 4' 7.464" E	82	310	22
159	21°13'18"N 86°01'24"E	41	300	5
160	21°13'18"N 86°01'24"E	35	301	5
161	21°13'18"N 86°01'24"E	50	266	10
162	21°13'18"N 86°01'24"E	75	310	3
163	21°13'18"N 86°01'24"E	50	278	19
164	21°13'18"N 86°01'24"E	50	250	7
165	21°13'18"N 86°01'24"E	52	303	2
166	21°13'18"N 86°01'24"E	37	290	5
167	21°13'18"N 86°01'24"E	76	188	8
168	21°13'18"N 86°01'24"E	63	153	6
169	21°13'18"N 86°01'24"E	52	270	18
170	21°13'18"N 86°01'24"E	77	176	5
171	21°13'18"N 86°01'24"E	52	270	1.5
172	21°13'18"N 86°01'24"E	88	355	1
173	21°13'18"N 86°01'24"E	62	114	9
174	21°13'18"N 86°01'24"E	61	110	6
175	21°13'18"N 86°01'24"E	75	330	1
176	21°13'18"N 86°01'24"E	74	145	1
177	21°13'18"N 86°01'24"E	65	45	3.5
178	21°13'18"N 86°01'24"E	74	320	4.5
179	21°13'18"N 86°01'24"E	75	175	6.5

Sl No.	Location	Dip amount (in degree)	Dip direction (in degree)	Thickness of Fracture (in cm)
180	21°13'18"N 86°01'24"E	65	95	3
181	21°12'55"N 86°01'46"E	60	100	25
182	21°12'55"N 86°01'46"E	70	110	30
183	21°12'55"N 86°01'46"E	70	130	0.5
184	21°12'55"N 86°01'46"E	82	120	0.5
185	21°12'55"N 86°01'46"E	65	90	11
186	21°12'55"N 86°01'46"E	55	180	16
187	21°12'08"N 85°58'20"E	42	55	21
188	21°12'08"N 85°58'20"E	35	50	18
189	21°12'08"N 85°58'20"E	41	125	4
190	21°12'08"N 85°58'20"E	30	75	2.5
191	21°12'08"N 85°58'20"E	47	305	1.5
192	21°12'08"N 85°58'20"E	54	255	2
193	21°12'08"N 85°58'20"E	53	251	2
194	21°12'08"N 85°58'20"E	60	360	14
195	21°12'08"N 85°58'20"E	25	105	4
196	21°12'08"N 85°58'20"E	60	170	3
197	21°12'08"N 85°58'20"E	60	80	4
198	21°12'08"N 85°58'20"E	62	230	7
199	21°12'08"N 85°58'20"E	55	223	10
200	21°12'08"N 85°58'20"E	56	174	3
201	21°12'08"N 85°58'20"E	65	300	3
202	21°12'08"N 85°58'20"E	60	315	2.5
203	21°12'08"N 85°58'20"E	61	185	4
204	21°12'08"N 85°58'20"E	54	180	3.5
205	21°12'08"N 85°58'20"E	54	255	2.5
206	21°12'08"N 85°58'20"E	30	173	3.5
207	21°12'08"N 85°58'20"E	69	345	3
208	21°12'08"N 85°58'20"E	35	20	4
209	21°12'08"N 85°58'20"E	54	360	8
210	21°12'08"N 85°58'20"E	36	155	2
211	21°12'08"N 85°58'20"E	30	115	3
212	21°12'08"N 85°58'20"E	28	76	3
213	21°12'08"N 85°58'20"E	50	200	1
214	21°12'08"N 85°58'20"E	55	300	2
215	21°12'08"N 85°58'20"E	65	15	6
216	21°12'08"N 85°58'20"E	57	335	6
217	21°12'08"N 85°58'20"E	50	0	15
218	21°12'08"N 85°58'20"E	60	295	2
219	21°12'08"N 85°58'20"E	31	30	10
220	21°12'08"N 85°58'20"E	40	305	12
221	21°12'08"N 85°58'20"E	50	290	12
222	21°12'08"N 85°58'20"E	60	300	4.5
223	21°12'08"N 85°58'20"E	50	300	4
224	21°12'08"N 85°58'20"E	84	95	9.5

Sl No.	Location	Dip amount (in degree)	Dip direction (in degree)	Thickness of Fracture (in cm)
225	21°12'08"N 85°58'20"E	35	295	20
226	21°12'08"N 85°58'20"E	40	290	17
227	21°12'08"N 85°58'20"E	46	105	3
228	21°12'08"N 85°58'20"E	45	105	4
229	21°12'08"N 85°58'20"E	58	305	14
230	21°12'08"N 85°58'20"E	55	110	5
231	21°12'08"N 85°58'20"E	40	115	4
232	21°12'08"N 85°58'20"E	48	123	14
233	21°12'08"N 85°58'20"E	60	135	13
234	21°12'08"N 85°58'20"E	68	95	9
235	21°12'08"N 85°58'20"E	55	156	3
236	21°12'08"N 85°58'20"E	60	184	3
237	21°12'08"N 85°58'20"E	45	147	5
238	21°12'08"N 85°58'20"E	78	75	12
239	21°12'08"N 85°58'20"E	61	145	6
240	21°12'08"N 85°58'20"E	46	270	7
241	21°12'08"N 85°58'20"E	55	140	3
242	21°12'08"N 85°58'20"E	40	270	2
243	21°12'08"N 85°58'20"E	35	267	2.5
244	21°12'08"N 85°58'20"E	34	300	3
245	21°12'08"N 85°58'20"E	40	315	3
246	21°12'08"N 85°58'20"E	50	295	4
247	21°12'08"N 85°58'20"E	38	285	4.5
248	21°12'08"N 85°58'20"E	70	135	4
249	21°12'08"N 85°58'20"E	43	292	3
250	21°12'08"N 85°58'20"E	50	295	5
251	21°12'08"N 85°58'20"E	50	273	7
252	21°12'08"N 85°58'20"E	85	120	2
253	21°12'08"N 85°58'20"E	70	133	4
254	21°12'08"N 85°58'20"E	70	142	4
255	21°12'08"N 85°58'20"E	35	295	2
256	21°12'08"N 85°58'20"E	42	215	2
257	21°12'08"N 85°58'20"E	70	313	19
258	21°12'08"N 85°58'20"E	58	55	2
259	21°12'08"N 85°58'20"E	30	302	5
260	21°12'08"N 85°58'20"E	75	143	2
261	21°12'08"N 85°58'20"E	60	118	8.5
262	21°12'08"N 85°58'20"E	87	120	8
263	21°12'08"N 85°58'20"E	70	143	6.5
264	21°12'08"N 85°58'20"E	71	145	2
265	21°12'08"N 85°58'20"E	54	141	7
266	21°12'08"N 85°58'20"E	65	58	3
267	21°12'08"N 85°58'20"E	65	220	1.5
268	21°12'08"N 85°58'20"E	58	135	2
269	21°12'08"N 85°58'20"E	50	355	6

Sl No.	Location	Dip amount (in degree)	Dip direction (in degree)	Thickness of Fracture (in cm)
270	21°12'08"N 85°58'20"E	70	145	2
271	21°12'08"N 85°58'20"E	60	105	4.5
272	21°12'08"N 85°58'20"E	50	150	10
273	21°12'08"N 85°58'20"E	60	140	4
274	21°12'08"N 85°58'20"E	68	150	6
275	21°12'08"N 85°58'20"E	85	65	8
276	21°12'08"N 85°58'20"E	60	65	6.5
277	21°12'08"N 85°58'20"E	48	40	4.3
278	21°12'08"N 85°58'20"E	80	135	15
279	21°12'08"N 85°58'20"E	70	80	4
280	21°12'08"N 85°58'20"E	75	135	20
281	21°12'08"N 85°58'20"E	75	135	5
282	21°12'08"N 85°58'20"E	72	95	7
283	21°12'08"N 85°58'20"E	76	142	4
284	21°12'08"N 85°58'20"E	62	132	12
285	21°12'08"N 85°58'20"E	65	330	7
286	21°12'08"N 85°58'20"E	68	278	7
287	21°12'08"N 85°58'20"E	84	145	3
288	21°12'14"N 85°58'49"E	81	50	2
289	21°12'14"N 85°58'49"E	30	42	8
290	21°12'14"N 85°58'49"E	69	280	14
291	21°12'14"N 85°58'49"E	65	68	1
292	21°12'14"N 85°58'49"E	72	115	22
293	21°12'14"N 85°58'49"E	45	75	3
294	21°12'14"N 85°58'49"E	68	135	3
295	21°12'14"N 85°58'49"E	70	130	5
296	21°12'05"N 85°01'52"E	45	95	18
297	21°12'05"N 85°01'52"E	42	100	12
298	21°12'05"N 85°01'52"E	33	80	13
299	21°12'05"N 85°01'52"E	69	155	4
300	21°12'05"N 85°01'52"E	84	225	5

CHAPTER 5

RESULT AND DISCUSSION

5.1 Result and Discussion

After detailed structural analysis of the study area around Anandpur, Keonjhar, Odisha, it shows that in this region quartz veins are intruded into the granitic rocks (Fig 4.2a-f) which comes under Singhbhum Granite phase III, after superimposing and co-correlation of satellite image with Stratigraphic Formation map. Superimpose of satellite image and the Stratigraphic Formation map are done after geo referencing. In this area the host granitic rocks are exposed to surface like plutons and fractures are developed into which number of veins are intruded. Veins are very often showing cross cut relationship but have seen with rarely any offsets. These offsets are generally developed when an early phase of vein is intersecting with the later phase of vein (Fig 4.2d). However, from the field observation it is clear that the major quartz veins are synchronous in nature. The veins range in width from a few millimeters to several centimetres. Quartz grains in the veins are showing phaneritic texture (clearly visible to the naked eye) and in pegmatitic veins diameter of quartz and feldspar grains are ranging from 4 mm to 10 mm.

Data on 235 quartz veins and 65 fractures orientations were gathered from the Anandpur region for the current investigation. Nonetheless, there are very a smaller number of widely distributed cracks in the host rock that are not filled with quartz vein. Although it is widely distributed, the maximum density is found in the NE-SW quadrant, which is aligned with the orientations of the veins and indicates that the fractures are preexisting fractures with veins emplaced into them. If the fracture orientations do not line up with the orientation of the veins, it can be assumed that these fractures aren't pre-existing fractures, and that this methodology isn't appropriate in that situation. Especially, the Bhimkund area has high density of unfilled fractures while Anandpur region has less density of unfilled fractures. From fig (5.1 a & b) It is seen that the NE-SW quadrant has the greatest number of both fractures and veins. There are three sets of quartz veins that are oriented N-S, NW-SE, and NE-SW. The rose diagram of the vein data indicates that the majority of the veins strike NE-SW. The stereoplot of these veins data reveals that the NE-SW striking

veins are dipping towards the SE quadrant. The contour map indicates that the veins' poles are most densely concentrated in the NW-SE region, and it displays a griddle distribution that shows a wide variety of dilated fractures. The zone of dilation is outside the ellipse and the zone of no dilation is interior of the ellipse. As fractures around σ_1 did not enlarge, so the σ_1 is located in the center of the ellipse. From the stereoplot and ellipse construction σ_1, σ_2, σ_3 direction and θ_1, θ_2, θ_3 is measured. θ angles are measured in stereo diagram from σ_1 to the edge of the ellipse along the semi major and semi minor axis. Measurement of θ_2 and θ_3 is taken along σ_1–σ_3 and σ_1–σ_2 plane respectively. The value of θ_2 and θ_3 comes out 17° and 34° respectively. From the equation (5) the stress ratio (ϕ) value comes out 0.72 and from the equation (6) the driving pressure ratio (R') is calculated, which is 0.91. The stress ratio indicates the shape of the stress ellipse, which is oblate strain ellipsoid and driving pressure ratio indicates high pore fluid pressure. The trend and plunge amount of σ_1, σ_2 and σ_3 were measured, which are 075° / 81.5°, 210° / 06° and 300° / 06° respectively.

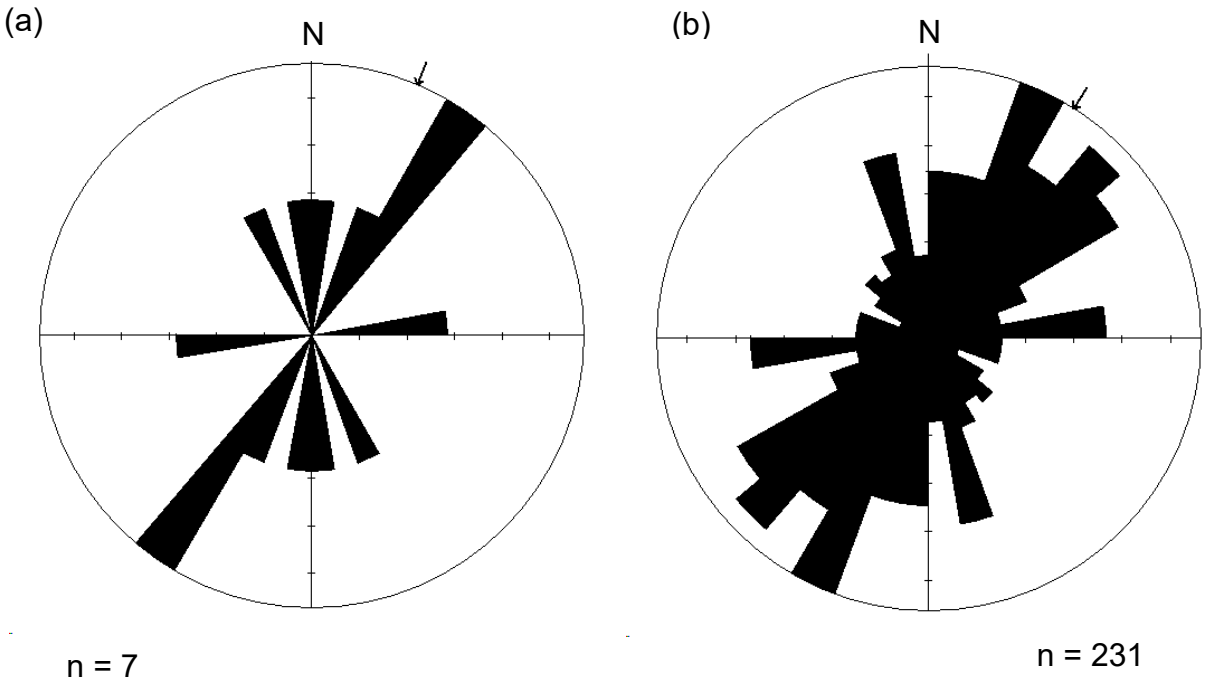

Fig 5.1: (a) Rose diagram of fractures data of Anandpur region which shows the most number of fractures are trending NE-SW. (b) Rose diagram of veins data of Anandpur region which shows NE-SW tend similar to the fractures.

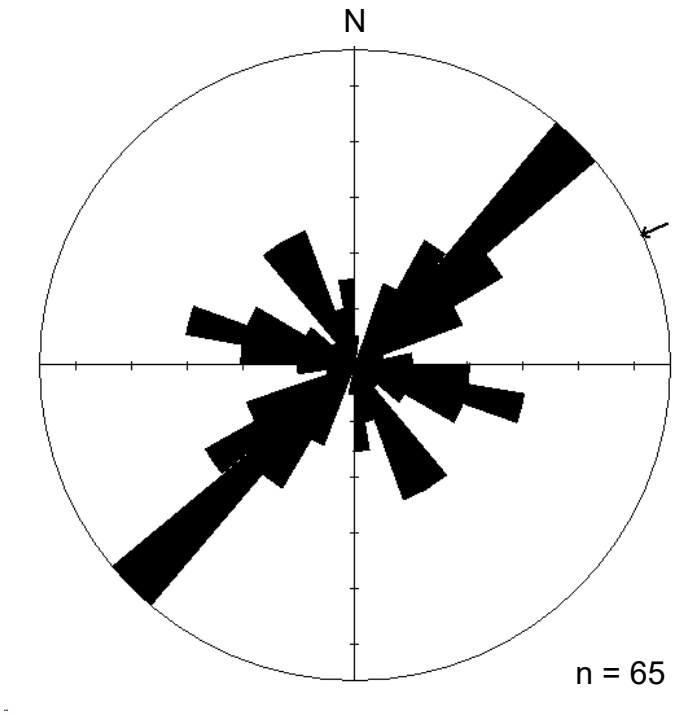

Fig 5.2: Rose diagram of fractures data of Bhimkund region which shows a general trend towards NE-SW.

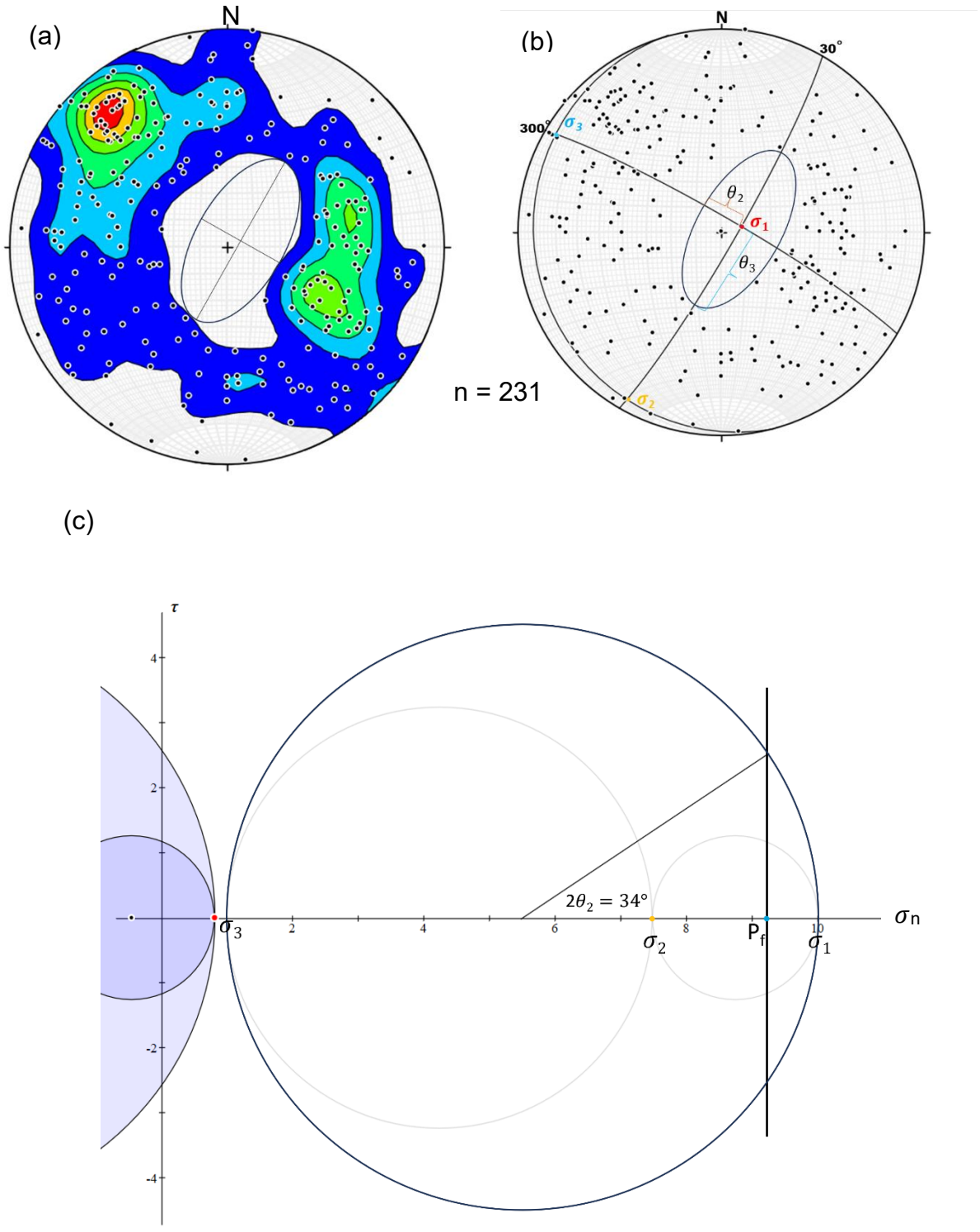

Fig 5.3: (a) Contour plot of all veins with the best fit ellipse drawn in the free space (b) Poles to veins with the best fit ellipse (c) 3D Mohr circle showing the relative stress value and the relation between pore fluid pressure and principal stresses.

3D Mohr circle provides the relationship between the fluid pressure and the fractures. Stereoplot shows gridle distribution and from the equation (5) and (6), it is noticed that $\sigma_2 < P_f < \sigma_1$. Because of this high fluid pressure

5.2 Conclusion

1. This study shows, θ_2 and θ_3 value is 17° and 34° respectively, and the trend and plunge amount of σ_1, σ_2 and σ_3 is 075° / 81.5°, 210° / 06° and 300° / 06° respectively.
2. By putting the above value in equation (5) and (6), the stress ratio (ϕ) and the driving pressure ratio (R') are calculated as 0.72 and 0.91 respectively.
3. The value of stress ratio which is 0.72, represents the oblate strain ellipsoid and the value of driving pressure ratio (R') which is 0.91, indicates the extensional regime as pore fluid pressure moves towards σ_2 from σ_3 in the mohr circle.
4. This study shows the fluctuation in pore fluid pressure (P_f) which controlled the quartz vein orientation and because of this fluctuation offsets are rarely seen.
5. On the basis of our result, we conclude that, these NE-SW trending fractures are formed in extensional regime and play a significant role in veins emplacement.

REFERENCES

Baer, Gidon, Michael Beyth, and Ze'ev Reches. "Dikes emplaced into fractured basement, Timna igneous complex, Israel." *Journal of Geophysical Research: Solid Earth* 99.B12 (1994): 24039-24050.

Bachhar, Priyanka, et al. "Mantle heterogeneity and crust-mantle interaction in the Singhbhum craton, India: New evidence from 3340 Ma komatiites." *Lithos* 382 (2021): 105931.

Bhatt, Sandeep, et al. "Pegmatite dyke emplacement and the state of stress during cratonization–An example from the Dharwar Craton (South India)." *Journal of Structural Geology* 123 (2019): 67-80.

Baer, G., Beyth, M. and Reches, Z. (1994) Dikes emplaced into fractured basement, Timna Igneous Complex, Israel.- Journal of Geouhvsical Research 99.24039-2405 I

Banerji, A. K. (1962). Cross folding, migmatization and ore localization along part of the Singhbhum Shear Zone, south of Tatanagar, Bihar, India. Economic Geology, 57, 50–71.

Biswal, T. K., & Sinha, S. (2003). Deformation history of the NW salient of the Eastern Ghats Mobile Belt, India. Journal of Asian Earth Science, 22, 157–169

Dey, Sukanta, et al. "Generation and evolution of Palaeoarchaean continental crust in the central part of the Singhbhum craton, eastern India." *Precambrian Research* 298 (2017): 268-291.

Delaney, Paul T., et al. "Field relations between dikes and joints: Emplacement processes and paleostress analysis." *Journal of Geophysical Research: Solid Earth* 91.B5 (1986): 4920-4938.

Dey, Sukanta, et al. "Mechanism of Paleoarchean continental crust formation as archived in granitoids from the northern part of Singhbhum Craton, eastern India." *Geological Society, London, Special Publications* 489.1 (2020): 189-214.

Dey, S., et al. "Early Crustal Evolution as Recorded in the Granitoids of the Singhbhum and Western Dharwar Cratons, Earth's Oldest Rocks." *Developments in Precambrian Geology*. Elsevier, 2019. 741-792.

French, Jason E., et al. "1891–1883 Ma Southern Bastar–Cuddapah mafic igneous events, India: A newly recognized large igneous province." *Precambrian research* 160.3-4 (2008): 308-322.

Friend, C. R. L. "AK Saha. Crustal Evolution of Singhbhum North Orissa Eastern India. Geological Society of India, Memoir 27, 1994. 341 pp. Price US $40." *Mineralogical Magazine* 59.397 (1995): 773-773.

Ghosh, Suranjan, et al. "A review of the Precambrian tectonic evolution of the Aravalli Craton, northwestern India: Structural, metamorphic and geochronological perspectives from the basement complexes and supracrustal sequences." *Earth-Science Reviews* 232 (2022): 104098.

Jolly, R. J. H., and D. J. Sanderson. "A Mohr circle construction for the opening of a pre-existing fracture." *Journal of Structural Geology* 19.6 (1997): 887-892.

Jain, Ashok Kumar, D. M. Banerjee, and Vivek S. Kale. *Tectonics of the Indian subcontinent*. Springer Nature, 2020.

Manikyamba, C., et al. "Boninitic metavolcanic rocks and island arc tholeiites from the Older Metamorphic Group (OMG) of Singhbhum Craton, eastern India: Geochemical evidence for Archean subduction processes." *Precambrian Research* 271 (2015): 138-159.

McKeagney, C. J., et al. "3-D Mohr circle analysis of vein opening, Indarama lode-gold deposit, Zimbabwe: implications for exploration." *Journal of Structural Geology* 26.6-7 (2004): 1275-1291.

Morfulis, Marcos, et al. "Quantitative spatial distribution analysis of mafic monogenic volcanism in the southern Puna, Argentina: Implications for magma production rates and structural control during its ascent." *Journal of South American Earth Sciences* 104 (2020): 102852.

Mondal, M. E. A., ed. *Geological evolution of the Precambrian Indian shield*. Springer, 2018.

Manikyamba, C., et al. "Mesoarchean gabbro-anorthosite complex from Singhbhum Craton, India." *Lithos* 366 (2020): 105541.

Mahapatra, Rasmi Ranjan, et al. "Style of fractional crystallization in basalts from the Paleoarchean western Iron Ore Group of Singhbhum Craton, Eastern India: implications from one atmosphere experimental studies." *Journal of the Geological Society of India* 98.5 (2022): 627-634.

Mondal, Tridib Kumar, and Manish A. Mamtani. "3-D Mohr circle construction using vein orientation data from Gadag (southern India)–implications to recognize fluid pressure fluctuation." *Journal of Structural Geology* 56 (2013): 45-56.

McKeagney, C. J., et al. "3-D Mohr circle analysis of vein opening, Indarama lode-gold deposit, Zimbabwe: implications for exploration." *Journal of Structural Geology* 26.6-7 (2004): 1275-1291.

Mukhopadhyay, Dhruba, and Abdul Matin. "The architecture and evolution of the Singhbhum Craton." Episodes Journal of International Geoscience 43.1 (2020): 19-50

Mondal, T.K., Mamtani, M.A., 2013. 3-D Mohr circle construction using vein orientation data from Gadag (southern India)–implications to recognize fluid pressure fluctua tion. J. Struct. Geol. 56, 45–56

R. Mir, Akhtar. 2022. ‘Proterozoic Newer Dolerite Dyke Swarm Magmatism in the Singhbhum Craton, Eastern India’. Geochemistry and Mineral Resources. IntechOpen. doi:10.5772/intechopen.104833

Roberts, S., R. P. Foster, and R. W. Nesbitt. "Mineralisation associated with early Precambrian basic magmatism." *Early Precambrian basic magmatism*. Dordrecht: Springer Netherlands, 1990. 157-188.

Schwab, Drew R., Tandis S. Bidgoli, and Michael H. Taylor. "Characterizing the potential for injection-induced fault reactivation through subsurface structural mapping and stress field analysis, Wellington Field, Sumner County, Kansas." *Journal of Geophysical Research: Solid Earth* 122.12 (2017): 10-132.

Sharma, Ram. *Cratons and fold belts of India*. Vol. 127. Springer, 2009

Saha, A., Basu, A. R., Garzione, C. N., Bandyopadhyay, P. K., & Chakrabarti, A. (2004). Geochemical and petrological evidence for subduction—Accretion processes in the Archaean Eastern Indian Craton. Earth and Planetary Science Letters, 220, 91–106

Sarkar, S. C. (2000). Crustal evolution and metallogeny in the Eastern Indian Craton. Special Publication of the Geological Survey of India, 55, 169–194

Sinha, K. K., et al. "Stratigraphic succession of Precambrian of Singhbhum: evidence from quartz pebble conglomerate." *JOURNAL-GEOLOGICAL SOCIETY OF INDIA* 49 (1997): 577-588.

Tiwari, Sudheer Kumar, and Tapas Kumar Biswal. "Palaeostress and magma pressure measurement of granite veins in the Neoproterozoic Ambaji granulite, South Delhi terrane, Aravalli–Delhi mobile belt, NW India: Implication towards the extension-driven exhumation of the middle–lower crustal rocks." *Journal of Earth System Science* 128 (2019): 1-13.

Valdiya, Khadg Singh. *The making of India: geodynamic evolution*. Springer, 2015.